Biomimetic materials to replace tubular tissues

Isabelle Martinier, Léa Trichet, Francisco M Fernandes

Biomimetic materials to replace tubular tissues

Isabelle Martinier, Léa Trichet[*] and Francisco M. Fernandes[*]

Laboratoire de Chimie de la Matière Condensée de Paris, Sorbonne Université, UMR7574, 4 Place Jussieu, 75005 Paris, France

Abstract

Repairing tubular tissues—the trachea, the esophagus, urinary and gastrointestinal tracts, and the circulatory system—from trauma or severe pathologies that require resection, calls for new, more effective graft materials. Currently, the relatively narrow family of materials available for these applications relies on synthetic polymers that fail to reproduce the biological and physical cues found in native tissues. Mimicking the structure and the composition of native tubular tissues to elaborate functional grafts is expected to outperform the materials currently in use, but remains one of the most challenging goals in the field of biomaterials.

Despite their apparent diversity, tubular tissues share extensive compositional and structural features. Here, we assess the current state of the art through a dual layer model, reducing each tissue to an inner epithelial layer and an outer muscular layer. Based on this model, we examine the current strategies developed to mimic each layer and we underline how each fabrication method stands in providing a biomimetic material for future clinical translation.

The analysis provided here, addressed to materials chemists, biomaterials engineers and clinical staff alike, sets new guidelines to foster the elaboration of new biomimetic materials for effective tubular tissue repair.

Abbreviations

Col[roman numeral]: type [roman numeral] collagen
dECM: decellularized extracellular matrix
EC: epithelial cells
ECM: extracellular matrix
Fn: Fibronectin
GI: gastro-intestinal
Hep: heparin
iPSC: induced pluripotent stem cells
Ln: laminin
PET: poly(ethylene) terephthalate
PEG: poly(ethylene) glycol
SMC: smooth muscle cells
UC: urothelial cells
USC: urine stem cells

1. Introduction

In living organisms, the transport of gases and liquids through the body is imperative to ensure homeostasis and, ultimately, the organisms' viability. These transport mechanisms occur at different length scales in living systems. On the lower end, at the nanometer scale, specialized transmembrane proteins like aquaporins enable molecule-by-molecule water transport between the cytoplasm and the extracellular environment. On the other end of the fluid transport scale, the meters' long circulatory system of humans handles an incessant pulsatile flow of several liters of blood. The radically different transport phenomena—defined by the properties of the fluid, its volume or its flow rate—require different driving forces. Osmotic forces drive water molecules across the cell membrane whereas blood is pumped by the mechanical action of the muscles in the cardiovascular system. A detailed analysis of the different strategies favored by evolution to cope with all fluid transport needs in biological systems, falls beyond the scope of this review article. However, if we focus on native, large-scale fluid transport systems—such as gastrointestinal and urinary tracts or respiratory and circulatory systems—they all share common features: a three-dimensional concentric arrangement of sublayers around a luminal space, lined by a tightly bound layer of cells named the epithelium. At a first glance, the diversity of fluid properties—gases, liquids with variable viscosities and semi-solids—seems to play only a small role in the strategies selected by evolution to transport large volumes of fluids. **Figure 1** highlights the common concentric layered structures of five different tubular organs, with detailed electron microscopy observations of their epithelium. It illustrates that, despite their different physiological functions, they share a large array of structural features—in particular three to four concentric layers, which compositions depend on each specific tubular organ[1] (Figure 1).

Tubular organs can adapt to some extent to moderate effects of stress[2], disease[3], aging[4,5] or environmental factors[6,7]. Clinical guidelines for the early treatment of damaged or malfunctioning tubular organs favor the use of drugs or other non-invasive procedures[8–11]. More severe cases require surgical replacement, using (a) autologous, (b) allogenic or (c) synthetic grafts. The most common procedure for tubular tissue grafting relies on allografts, *i.e.* native tissues harvested from another patient or obtained from a donor bank[12]. However, their availability is limited, either due to technical limitations to preserve the tissues on the long term, or due to plain shortage of suitable organs[13]. Synthetic tubular grafts are a promising solution to tackle these limitations, in particular because they are independent from most logistics limitations. Since the first grafts developed for vascular purposes using PVC (Vinyon) cloth in 1952[14], research efforts have extended this concept to a wide range of other synthetic polymers. Prosthetic grafts from polytetrafluoroethylene (PTFE (Teflon®), extruded PTFE (Gore-Tex®)),

polyethylene terephthalate (PET (Dacron®)), or polyurethane (PU) have produced fruitful results as cardiovascular grafts, in particular for the replacement of large-diameter vessels (with an internal diameter above 6 mm)[20]. However, the unsatisfactory long-term clinical results (Patency and viability, anastomotic leakage, obstruction of the grafts such as thrombus or stenosis[12]) and the mismatch between the mechanical and biological properties of the living tissue and of those of the implanted biomaterial[15], have directed research towards alternative routes. Among these new approaches, biomimetic materials are expected to play a central role.

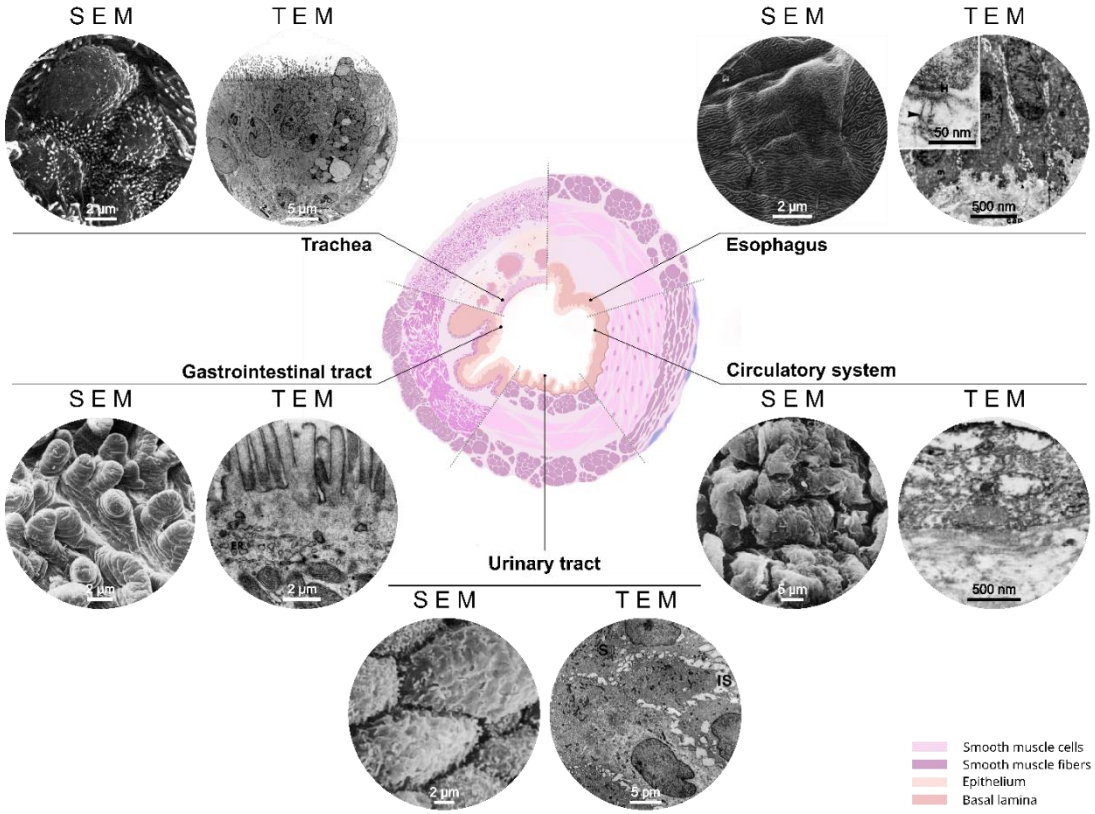

Fig 1. Similarities in the structural and compositional features across different tubular tissues. Center, schematic histological transversal cross-sections, associated with scanning electron microscopy (SEM) and transmission electron microscopy (TEM) images of epithelia for each tissue. **Trachea,** *chicken* (For tracheal epithelium electron microscopy observations, biopsies sourced from camel[296], rats[297], dogs[298] and porcine[299] were found, but not from humans.): (SEM) group of mature goblet cells on the luminal surface, exhibiting sparse microvilli on the peripheral surface[16]. (TEM) a mature goblet cell with a characteristic goblet shape releasing mucous granules (G) into the lumen of the trachea through pits or pores[16]. **Esophagus**, *human*: (SEM) individual squamous epithelial cells are separated by distinct intercellular ridges, and covered by varying arrangements of distinct micro-ridges forming a latticework[17]. (TEM) at low magnification, basal cells attached to the basal membrane (arrow heads) with hemidesmosomes (H). Nucleus (n) and intranuclear mitochondria (m) are observed. The inset at higher magnification details the basal membrane and shows anchoring fibrils (arrow heads) running into the lamina propria[18]. **Circulatory system**, *human*: (SEM, *saphenous vein* and TEM, *coronary artery*) high magnification of the luminal surface of a saphenous vein, ridges are covered with smooth-surfaced endothelium[19]. **Urinary tract**, *various origins*: (SEM, *human*) the transitional epithelium in the upper part of the prostatic urethra. Among the typical apices of the superficial cells, small apices provided with microvilli emerge[20]. (TEM, *sows*): basal cells (B), intermediate cells (I) and a few vesicles at the apical

portion of cytoplasm close to the basal membrane (arrow)[21]. **Gastrointestinal tract**, *human*: (SEM) the majority of villi are fingershaped, but occasional bifid and leaf-shaped villi can be easily recognized[22]. (TEM) apical cytoplasm of absorptive cells on a single villus located at the tip extremity, showing the length variations in the micro-villus lengths and the reticulum (R)[23].

The literature offers a wide range of definitions to the notion of biomimetic materials. Taken in a strict sense—as we do herein—a biomimetic material corresponds to an artificial material which structure and composition reproduces that of a natural tissue. Intuitively, reaching a high degree of similarity with a native material in its compositional and structural aspects, maximizes the chances that it equals its functions. For instance, in the case of gastrointestinal regeneration, it has been shown that cells attach and proliferate at a higher rate on biologically-based supports (biopolymers or ECM-derived materials) than they do on artificial ones[24]. This approach has resounding implications in the context of bioengineering and evidence of enhanced biointegration and low immune response of biomimetic materials has now been established in the medical field[25]. As a consequence, a detailed analysis of their anatomical structure, their composition and the relevant cell types, provides solid guidelines to conceive materials whose properties (mechanical, fluid transport, biocompatibility, etc) are comparable to those of original tissues and organs[15].

Despite their different physiological function, tubular organs share a large array of structural features—in particular three to four concentric layers, which compositions depend on each specific tubular organ (Figure 1)[1]. On the luminal side of tubular organs, cells adhere and form a tissue-specific epithelium that acts as a semipermeable interface between the transported fluid and the inner tissue wall. In the middle layer, smooth muscle cells—the effectors of motility—mediate the contraction of the lumen under specific physical or biological signals[26]. The outer layer provides mechanical support to the overall structure and favors the biochemical crosstalk between the implanted materials and their environment. In the outer layers, cells are embedded in the extracellular matrix (ECM), composed of macromolecules that include type I and IV collagens, elastin, proteoglycans and glycoproteins (laminin, fibronectin and nidogen). Each layer is composed of a different combination of components that determine the type and the density of binding sites that direct cell behavior. Type I collagen, the major component of the ECM in mammals, acts as a structural backbone for the whole tissues and as a support for cell adhesion, whereas elastin provides the tissues with resilience and elasticity[27].

Beyond type I collagen, other components play central roles in native tissues—laminin and fibronectin are involved in cellular adhesion and migration, and nidogen mediates biological responses of cells to laminin. In addition to the proteins mentioned above, proteoglycans ensure tissue hydration as well as an array of specific biological roles[28]. Despite the common traits between different tubular organs—that will be discussed further as a rationale for the elaboration of biomimetic grafts—the layers' composition is specific to each tissue[1].

The collective work of clinicians, biologists, materials chemists and physicists led to the creation of a variety of tubular grafts. The fabrication techniques involved in the elaboration of these materials can be classified according to their structure and composition, on a two-axis graph. The *biomimetic structure* axis refers to the degree of success in reproducing an adequate physical environment for cell colonization (macroporosity)[29] and the relevant number of concentric layers able to reproduce the macroscopic tubular arrangement of the tissue. The *biomimetic composition* axis refers to the level of reproduction of the ECM composition, which determines interactions with cells. **Figure 2** depicts the wide spectrum of tubular biomaterials covered by the current fabrication techniques, which will be developed below (sections 2; 3). In addition, Figure 2 provides guidelines for the conception of future biomimetic grafts, while introducing currently developed techniques.

If biomimetic materials appeal for their capacity to recapitulate the structure and function of the native tubular tissues, the current panorama of materials is much broader. **Figure 2** depicts the main processing strategies, composition and geometry of the materials developed for tubular tissue engineering. Synthetic polymers are extremely versatile in their composition yet easily reproducible, which leads, respectively, to adjustable properties and steady quality[30]. These provide a high level of control over the mechanical properties, the cell spatial arrangement and differentiation by textural or topographic cues[31]. However, in the context of implantation procedures, synthetic scaffolds fail to recruit cells from anastomosis regions or from the surrounding environment due to the lack of specific cell-adhesion sites[12]. This results in poor cell proliferation substrates[17], with poor or absent epithelium. In addition, one should consider the possibility of materials to degrade *in vivo,* altering their structure and interactions with cells[32]. Polymers commonly used include polymethyl methacrylate (PMMA), silicones, polyvinyl chloride (PVC) and polyethylene terephthalate (PET), among others[33]. Polyesters and polyurethanes have also been investigated as replacement materials for the small intestinal submucosa, the esophageal submucosa, the gastric acellular matrix, or the aortic acellular matrix[34]. Current synthetic devices are now shifting from prosthetics towards scaffold materials to favor regeneration of tissues and long-term biocompatibility, by using biodegradable polymers such as: poly-lactic acid (PLA), polyglycolic acid (PGA), poly-l-lactic acid (PLLA), their copolymer poly(lactide-co-glycolide) and polycaprolactone (PCL)[35]. Another alternative route is to take benefit of the mechanical properties of synthetic polymers, and combine them to biologically derived components to enhance their biocompatibility. Entangled networks of PMMA and type I collagen, generated by co-electrospinning, provide a higher number of cellular anchoring sites that favors biointegration[36]. The addition of a biomimetic coating using proteins from the basal membrane—type III and IV collagens, fibronectin, laminin[37,30]—or the addition of active biomolecules[38] equally enables higher recruitment and adhesion rate of epithelial cells.

Alternatively, biomaterials exclusively elaborated from ECM components, have proven efficient in promoting cell adhesion, proliferation and morphogenesis[39], ultimately leading to enhanced biointegration. In such case, the material performances depend mostly on the use of native biological components to reconstitute the tubular wall composition, and less on the structural and textural features of the material.

In this review, we describe the requirements to reconstitute the complexity of the native tissues, based on a thorough analysis of their specific biological and structural features (section 2), and we provide an overview of the existing methods to synthesized tubular tissue-analogs (section 3). We anticipate that the tissue-centered vision that we offer, restricted here to hollow architectures, will shift how the scientific community envisages the elaboration of new, more clinically-relevant biomimetic materials.

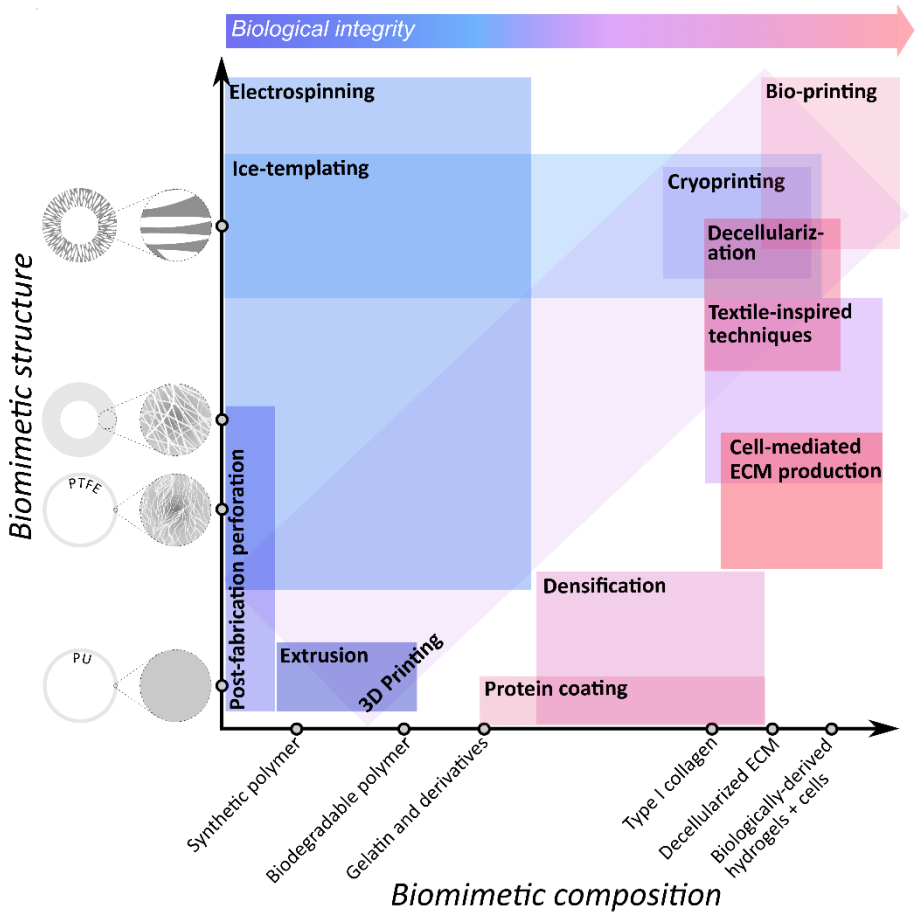

Fig. 2. Strategies to engineer biomimetic tubular tissues. Blue boxes refer to techniques for which the integrity of biological entities is hindered due to processing in the synthetic or biologically-derived composition. Pink-red boxes refer to techniques that preserve biologically-derived components, from biomolecules up to cells.

2. Structure and composition of tubular tissue layers

A detailed analysis of the native tissues enables to understand how each component holds a peculiar role in the tissues' structure and composition, giving guidelines for fabricating biomimetic materials that effectively replace damaged tissues. As mentioned above, tubular organs are multilayered structures, composed of three to four concentric layers, with specific cell arrangements and ECM architectures depending on their physiological function[40] (Figure 1). In the innermost layer, epithelial cells cover the lumen to form acellular sheet, the epithelium. Cells are anchored on a thin basal membrane, which separates the epithelium from the outer layers. Outer layers are populated by various type of cells—fibroblasts, nerve cells, smooth muscle cells, among others, depending on the tissue—embedded in a protein-rich extra-cellular matrix. This arrangement can be depicted by a dual-layer model consisting of an epithelial inner layer and a muscular outer layer. Table 1 details the biological and physical properties of each of those simplified layers (epithelial and muscular layers) of tubular tissues, including the circulatory system, the trachea, the gastro-intestinal tract, the esophagus, and the urinary tract.

Following what was introduced above, **Table 1** highlights the predominance of type I collagen in the composition of tubular tissues. The structural conformation of collagen and its hierarchical arrangement are responsible for the anisotropy of tubular tissues and for their elastic properties[41], necessary to fulfill their physiological functions. *In vivo*, type I collagen can be described by four hierarchical levels: the amino-acid sequence, the triple helix (collagen molecule), the fibrils and the suprafibrillar structures. Generated by cells, amino-acids sequences self-assemble into triple-helices in the intracellular space and form fibrils upon extrusion from the cytoplasm. Interfibrillar proteoglycans, orthogonal to fibrils, bound them together to form fibers[42]. Fibrils display a typical staggering that results in an axial characteristic distance of 67 nm, named D-spacing, and observable exclusively under electron microscopy or by X-ray diffraction. Fibrils are arranged in higher ordered structures whose architecture are specific to each tissue (bone, skin, tendon…)[43]. These arrangements in tissues have been widely explored by microscopy techniques, in particular by TEM and polarized light microscopy[44]. The latter revealed a liquid crystal-like behavior, with the formation of lyotropic mesophases associated with specific tissues (cholesteric, nematic, plywood, among others)[45–47]. Mimicking *in vitro* the native motifs found *in vivo* requires a deep understanding of the physico-chemical conditions governing its emergence, notably during the fibrillogenesis step that encompasses the transition from acid solution to a fibrillar gel. However, the necessity of a high collagen density, and the structural modifications of collagen during the fabrication processes have received little attention and are most often disregarded in the literature. *In vitro*, fibrillogenesis can be triggered by increasing the pH or ionic force, collagen molecules are stabilized into fibrils that present the characteristic D-banding native fibrillar pattern of 67 nm[48]. Besides the use of soft fibrillogenesis pathways, a large part of the research using collagen relies on the use of chemical cross-linkers (EDC, genipin

and glutaraldehyde), or physical treatment (dehydrothermal or UV treatment). However, controversy exists regarding the use of chemical crosslinkers. Bonds formed between collagen molecules differ from a cross-linker to another one[49], resulting in various biological responses that may not be conducive to tissue regeneration. Their potential toxicity and immunogenicity, even at low concentrations, has been reported to reduce cell proliferation and adhesion *in vitro*[49]. Physical treatments tend to denature collagen, forming gelatin that hinders the reformation of native-like fibrils. Despite the predominance of type I collagen in tissues, using it as a building block in tissue engineering requires a precise control over the elaboration conditions, to avoid its degradation that results in poorly biomimetic materials.

Table 1. Structural and compositional properties of tubular tissues based on a dual-layer model composed of an epithelial layer lining a muscular layer.

Tubular tissue in the human body	Epithelial inner layer		Muscular outer layer		Refs.
	Biological properties	Physical properties	Biological properties	Physical properties	
Circulatory system	*Endothelium*: endothelial cells aligned in the direction of the blood flow. *Basement membrane*: basal lamina[50], mainly	*Permeability*[*]: at a steady state, junctions in ECs originating from arteries and micro-vessels are tighter than those originating from veins. Diffusion distances of FITC-dextran deposited on monolayers of unstimulated cells, are reported at 8,3 % (arteries), 10,2 %	*Cells*: contractile SMCs, spindle shaped, and arranged circumferentially in a spiral shape within the matrix. On the outer part, a few fibroblasts and fibrocytes maintain the plasticity of the	*Ultimate tensile stress*: for the adventitia, 1,430 ± 604 kPa (circumferentially) and 1,300 ± 692 kPa (longitudinally). For the media, 446 ± 194 circumferentially and 419 ± 188 kPa longitudinally[51].	50 to 55

[*] Caution should be taken with the permeability assessments. The measurement of epithelial permeability is an indicator of the tightness of the cellular network, necessary to withstand the physiological intraluminal pressure while allowing for molecular exchanges. *In vivo* direct measurement of arterial permeability is a procedure that is impossible to be done without harming patients. Hence, *in vitro* models have been developed to obtain an approximation of it, but the physiological micro-environment has not been fully reconstituted yet. For instance, permeability values show heterogeneity between different phenotypes of human ECs *in vitro*[83]. The EC permeability response upon stimulation with histamine, platelet activator factor (PAF), and thrombin is also modulated by the cells' origin[83]. The static conditions often used in the current models also influence junction response to stimuli. The use of thrombin or other permeability modulator can affect actin cytoskeleton, resulting in large gap junctions slowly forming overtime, compared to the discrete and rapid endothelial gaps observed *in vivo*. Finally, endothelial cells upregulate inflammatory genes in culture conditions, which might bias results. The permeability of vascular endothelium is a delicate measurement, and the value must not be taken as an absolute but be mitigated by the experimental conditions[59].

	composed of type III and IV collagens, along with laminin isoforms, entactin and fibronectin (see section ***2.1.2*** for more details).	(micro-vessels) and 15,8 % (veins) of the total wall thickness after 1 h. *Ultimate tensile stress*: in intima, 394 ± 223 kPa circumferentially and 391 ± 144 kPa longitudinally[51]. *Stiffness*: mean stiffness values in intima layer of human aorta is 24.04 ± 13.97 kPa, measured by AFM. Intimal collagen fibers stiffness was also measured by ultra-AFM and evaluated at 7.31 ± 3.5 MPa[40]. Collagen fibers angle[3]//***: 15.2° in the intima, with respect to the vessel axis[52].	arterial wall, which allows remodeling upon mechanical stress or biochemical stimuli[53]. *ECM*: fibrous, contains collagen, elastin and proteoglycans, in which SMCs are embedded. Tunica media is isolated from the other layers by elastic laminae[54]. The adventitia is a connective tissue composed of a dense network of collagen and elastin fibers arranged along the vessel axis. This layer is infiltrated	*Compliance*: average large and small arterial elasticity of 12.9 ± 4.2 mL/mmHg x 10 and 4.4 ± 2.3 mL/mm Hg x 100, measured on human patients [55]. *Stiffness*: for the *media* of human aorta the stiffness is 22.18 ± 5.54 kPa, and for the *adventitia* 22.54 ± 3.35 kPa[55]. *Collagen fibers angle*[†]: 28.8° for the media and 57.1° for the adventitia, with respect to the vessel axis[52].	

[†] Collagen fibers angle is an important feature of tissue, which guides cells migration along the axis of the fibers and provide binding sites. This angle particularly important in arterial tissue where collagen fibers have a circumferential arrangement.

			with nerve fibers, lymphatic vessels, and the vasa vasorum.		
Trachea	*Epithelium*: pseudostratified ciliated epithelium containing ciliated cells (over 50 %), goblet cells, basal cells and neuroendocrine cells40,[57]. *Basement membrane*: collagen type IV, V and laminin in the upper part (*lamina densa*), secreted by the epithelial cells. Fibronectin, type III and V collagens are secreted by subepithelial fibroblasts in the thicker *lamina reticularis*[58].	*Permeability*: $1.05.10^{-14}$ $m^4.N^{-1}.s^{-1}$ towards water in porcine hyaline cartilage[59]. *Stiffness*: no data was found in the literature for tracheal apical surface stiffness. Eventually, stiffness of cultured lung epithelial cells seeded on petri dish was reported at 8.70 ± 0.23 kPa by AFM[60]. *Mucus viscosity*: from 0,01 to 1000 Pa.s for healthy human tracheal mucus. Pathological conduits often lead to increased viscosity values[61].	*Cells*: smooth muscle cells. ECM (*submucosa* and *adventitia*): connective tissue rich in elastin that also contains seromucous glands and cartilage rings. Horseshoe-shaped rings of hyaline cartilage (type II collagen and chondroitin sulfate) from the submucosa are encased.	*Ultimate tensile stress*: longitudinal elastic modulus of 1.10 ± 0.68 MPa for porcine tracheal ring[62]. Circumferential elastic modulus of 4.6-13.6 MPa for human trachea. *Compliance*: ranging from 0.046 to 0.101 $cm.H_2O^{-1,}$ measured on a handmade setup. Sections were fixed and pre-strained, then pressure response to intraluminal injection of Dulbecco's PBS was measured[63]. *Stiffness*: tensile stiffness of cartilage from human tracheal sections varies from 1.8 ± 2.1 MPa to 10.1 ± 3.3 MPa depending on the age (17 to 81 years old), water content, and is inversely proportional to collagen content. The outer layer provides the higher stiffness (14 MPa) compared to the innermost layer (5 MPa)[64].	57 to 64

Gastro-intestinal (GI) tract (stomach, large and small intestines, rectum)	*Epithelium*: simple columnar epithelium composed of enteroabsorptive cells, goblet cells, Paneth cells and neuroendocrine cells. The concentration of the mucus on the epithelium was reported at 19.9 ± 0.8 % (w/w) for human ileal mucus[65]. *Basement membrane*: mucosal folds and finger-like vili structures[66].	*Permeability*: in the case of the GI tract, it relates to the porosity of the mucus (up to 200 nm diameter in purified porcine jejunal mucin network[65]). However, in human ileal mucus, 58.1 ± 4.7 % of 500 nm latex beads dispersed in bile salt at a physiological concentration (11 mM) are able to diffuse. Permeability of the mucus is thus not only depending on the pore size, but also on the interactions between the mucus and the diffusing particles and the structural organization of the mucus. A model proposes that small non-mucoadhesive particles can diffuse through lamellae and create transient channels though which bigger particles can pass[65]. *Stiffness*: for colonic tissue and the ileum (a section of the small bowel), stiffness is respectively of 0.698 ± 0.463 kPa and 0.641 ± 0.342 kPa. Values were measured by a custom-cantilever based indenter[67]. *Mucus viscosity*: mean viscosity of 23.4 ± 8.2 mPa.s[65].	*Cells*: smooth muscle cells. ECM (*muscularis mucosa* and *adventitia* or *serosa*, depending if the gut is extra- or intra-peritoneal): vascularized tissue divided into longitudinal and circular muscle fiber layers[68], lying on the submucosa, a connective tissue containing type III collagen[69].	*Ultimate tensile stress and strain*: 0.57 ± 0.12 MPa transversally and 0.677 ± 0.19 longitudinally on surgically resected human stomach, with a maximum strain of 190 % for both[70]. *Compliance*: 1.49 ± 0.15 $mL.mmHg^{-1}$ measured for canine ileum[71]. *Stiffness*: 0.641 ± 0.342 kPa measured for bovine ileum and 0.698 ± 0.463 kPa for bovine colon[67].	65 to 71

Esophagus	*Epithelium*: stratified squamous epithelium. *Basement membrane*: *lamina propria* and *muscularis mucosae* contains gland cells, endocrine cells, small blood vessels, nerve fibers and lymphatic cells. It is surrounded by the submucosa layer which contains areolar connective tissue, blood and lymphatic vessels, and nerve fibers[72].	*Permeability*: for healthy epithelium, biotin diffuses only into the superficial layers at a distance of 8.3 % ± 2.4 % to the lumen, compared to 100 % diffusion in the case of chronic epithelial inflammation (eosinophilic esophagitis)[73]. *Stiffness*: no data was found in the literature for esophageal apical surface stiffness. Data were only found for cells cultured on synthetic substrates. *Opening angle*‡: 134.3 ± 19.1° measured for rat esophageal mucosa.	*Cells*: the upper third of the esophagus is composed of striated muscle cells, and on the lower third of smooth muscle cells. *ECM (muscularis externa and adventitia)*: thick muscle layer consisting of an inner and outer longitudinal layer, separated by a nervous layer (*myenteric plexus*). The outer layer contains blood vessels, veins and lymphatic vessels[74].	*Ultimate tensile stress and strain*: for human esophagus maximum stress is 1.2MPa and destructive strain is 140 %[70]. *Compliance*: mean value of 2.27 % volume/mmHg for children esophagi[75]. *Stiffness*: 2.24 ± 0.39 kPa and 12.2 ± 70.78 kPa in the circumferential and longitudinal directions for rat esophagus[76]. No data was found in the literature for human esophagus. *Opening angle*[4]: 62.2 ± 7.0°, measured for intact rat esophagus.	72 to 76

‡ The opening angle is a particularly relevant measurement of esophageal tissue. It is an indicator of the cartilaginous flexibility and the ability of the material to deform for swallowing purposes.

Urinary tract (ureter, urethra)	*Urothelium:* transitional epithelium for ureter, pseudostratified columnar and transitional epithelium for urethra. The epithelium is populated by a single layer of umbrella cells, followed by intermediate cells and a basal cell layer[77]. *Basement membrane (lamina propria):* loose connective and vascularized tissue with many elastic fibers.	*Permeability*: no data was found for urinary tube. The same urothelium lines ureter, urethra and the bladder, hence we herein assume their properties equivalent. For the bladder, permeability to water and urea were estimated at P_D = 4.12 ± 0.29.10^{-5} cm.s^{-1} and 4.35 ± 0.65 .10^{-6} cm.s^{-1}. For smaller species like ammonia and protons, permeability values of 5.00 ± 0.48.10^{-4} cm.s^{-1} and 2.96 ± 1.86.10^{-3} cm.s^{-1} were measured. The epithelium only contributes for 80 % of the resistance to water flow and over 95 % of the resistance to fluxes of urea, ammonia, and protons[78]. *Stiffness*: 31 ± 0,5 Pa for the apical surface of mouse bladder urothelium, measured by AFM[79].	*Cells (mesothelium)*: layer of epithelial cells covering the *serosa*. *ECM (serosa, the visceral peritoneum)*: areolar connective tissue for ureter, and muscular layers (one longitudinal and one circular) for urethra.	*Stiffness, tensile stress and strain*: no data was found in the literature for urinary tubes, research focuses mainly on the bladder. *Compliance*: maximal urethral opening of 0.35 ± 0.2 mm²/cmH_2O for human[80].	77 to 80

2.1 Epithelial inner layer

The innermost surface of the tubular walls consists of an epithelium—a tight layer of cells—that covers the thin basal membrane of the lumen. Epithelia are widely spread throughout the body, covering most organs and body surfaces. They isolate the tissues from non-self or any other substances in the lumen, prevent direct contact of blood with ECM to avert thrombosis, and favor pathogens' evacuation[81]. Sensors and specific receptors at the cell surface participate to immune defense by generating host-pathogen signaling cascades, and maintain homeostasis. Depending on its permeability, the epithelium also allows exchanges with its environment[82].

The classification of epithelia is based upon cell organization (orientation and number of cell layers) and cell shape. Four types of organizations are commonly considered[81]. Simple epithelium consists in a single layering of tightly-bound cells. Oppositely, stratified epithelium is composed of two or more cell layers, with equivalent size and morphology. In pseudostratified epithelium, a single layer of cells covers the surface, but uneven cells' shape and size creates a layered or stratified effect. Transitional epithelium is a stratified epithelium, for which cell morphology adapts following the organ distention. For instance, under low pressured fluid cells are cuboidal, whereas if pressure increases they flatten and adopt a squamous morphology. In columnar epithelia, elongated cells arise from the basal membrane to the exposed surface in a compact arrangement. These cells often express motile projections named cilia on their surface, consisting in two central microtubules, encompassed by nine microtubule doublets. These small hair-like structures increase the sensitivity to fluid pressure and flow, and can move in coordinated waves to propel mucus or other fluids and eliminate foreign substances[57]. Permeability, one of the key functions regulated by epithelia, depends on the cellular arrangement and junctions mentioned above, in order to provide proper supply to the adjacent tissues' physiological needs.

Epithelial cells' shape and arrangement reflect the epithelium functions at a given site. Under the passage of blood, epithelium (namely endothelium) adopts a *simple squamous* structure. It acts as a semi-permeable barrier for rapid diffusion of gases or materials through cells membranes or junctions[83]. In gastro-intestine tract, *simple columnar* epithelium is responsible for the absorption and secretion of mucus and enzymes. Nutrients absorption is maximized by topographical specifications associated with increased surface area: mucosal folds, finger-like villi and columnar crypts[57]. The luminal surface is protected from damage by a mucin layer, responsible for lubrication, which is secreted by goblet cells[56]. In the GI tract, a deleterious consequence of loose epithelial cell junctions is increased permeability from the lumen, resulting in paracellular transport of water, nutrients and ions. In trachea, a single layer of columnar cells of various heights and shapes lines the lumen, giving the appearance of stratifications. This *pseudo-stratified* structure favors the entrapment of foreign particles (bacteria, pollutants) in the mucus. Cilia on the surface of the cells contribute to move the contaminated mucus out of the airway. Damaged or senescent cells are renewed by reserve cells migrating from the basal lamina to the mucosal

surface. The tubular structures exposed to higher distension and stretch—esophagus and urethra—are endowed with multiple layers of cells that collectively form a *stratified squamous* epithelium. The extended number of cell layers limits the diffusion from and into the underlying tissue, and it prevents erosion by acidic food and urine[81]. The constant replacement of cells ensures the dynamics required for repairing epithelial damages and the subsequent restoration of the physiological permeability. The epithelium of urethra and ureter, urothelium, differs slightly from those previously mentioned, since it needs to accommodate significant distension and stretch. Cells exhibit various shapes in their constitutive layers, forming a *transitional epithelium*. Thicker layers and tight arrangement of cells separate more efficiently the basal lamina from outer substances that might be toxic such as waste in urine. The thickness of the cellular layer and arrangement of cells in urothelium makes it almost impermeant under physiological conditions[56,84,85].

In native tissues, discriminating the mechanical properties of the cellular layer from those of the underlying tissue is technically challenging. It is however commonly accepted that the epithelial layer contributes poorly to the mechanical properties of tubular tissues. Lu *et al.* measured the radial Cauchy strain along a porcine coronary artery, and demonstrated that it increases gradually from the inner to the outer layers, as both smooth muscle cells and collagen fibers present in the latter absorb the deformation[66]. A sounder criterion to evaluate the physical properties of each type of epithelium relies on measuring the permeability of the cellular junctions and their resistance to hydraulic pressure. The respective data for each epithelium is reported in Table 1.

In vivo, re-epithelialization is vital for repairing damaged tissue. This process is mediated by different types of cell junction types: tight junctions, anchoring junctions, and gap junctions[85]. Tight junctions are responsible for the impermeability of the cellular layer by preventing intercellular infiltration. Anchoring junctions stabilize cells and allow cellular adaptation to mechanical or geometrical cues through lateral and basal connections: desmosomes (cell-cell link though cadherins), hemidesmosomes (cell-ECM link through integrins) and adherens (cell shape regulation due to intracellular link to actin cytoskeleton)[85]. The essential component of endothelial junctions, VE-cadherin, forms Ca^{2+}-dependent, homophilic interactions between adjacent endothelial cells to maintain a tight endothelial barrier[86]. Gap junctions are intercellular communication channels, through which ions and small molecules travel whereas macromolecules can cross the endothelial barrier in three ways: (1) between the cells, through cell junctions (paracellular); (2) through the EC, via pores (diaphragms or fused vesicles); and (3) transcellularly, via shuttling vesicles and specific receptors[86].

The type of cells that line the luminal part of tubular organs and their arrangement largely dictate the function of epithelia in each organ. Although cell-cell interactions are qualitative markers for the functionality of the epithelium there is an equally important aspect that determines the quality of this cell layer: the underlying support materials. The following section addresses the composition and the

organization of the basal membrane (BM), the underlying supporting materials onto which epithelial cells adhere.

2.2 The interfacial layer: the basal membrane

The basal membrane is a thin and dynamic layer that separates the epithelium from the rest of the connective tissue. The BM is composed of tissue-specific proteins isoforms that dictate the phenotypes of cells able to anchor[87]. It is a critical layer for the formation of the epithelium, and it is also involved in its regulation and maintenance through biochemical signaling (hormones, growth factor, cell adhesion ligands) and mechanical support (roughness, pore size, tensile modulus).

Despite its small thickness ranging between 50 to 300 nm, the BM is structured in two distinct layers, the basal lamina—composed of the *lamina lucida* and the *lamina densa*—and the *lamina reticulata*. Fibrillar type IV collagen and laminin isoforms dominate the composition of the BM. Nidogen (also named entactin), perlecan, fibrinogen and fibrin, act as linkers between collagen and laminins to form a fibrillar network, often in the form of a 2D random mesh[88]. Interconnected pores cross the full thickness of the BM, and allow for the transport of solutes and for the transmigration of cells without requiring matrix degradation or remodeling. As an example, the tracheal basal membrane features an average density of 737–863 pores/mm² with a mean diameter of 1.76 µm[50]. Mechanical properties of the BM vary with age, medical condition, anatomical site and species. Furthermore, the spatial heterogeneity in BM mechanical properties direct the cellular behavior locally and, at a larger scale, drive the tissue morphogenesis or expansion[89]. At the tip of a growing lung for instance, the alternance of a thicker region followed by micro-perforations and thinning in the BM promotes branching and cell proliferation. The thicker region—built by a rearward translocation of the BM—stabilizes and constrains the expansion, while at the growing tip, the perforations and thinning locally increase the compliance to facilitate the expansion of both epithelium and BM[90]. Combined with the topography, the BM also influences cell function and phenotype. For instance, in the intestine, the luminal surface is structured in finger-like projections (or villi, 0.5-1.2 mm in height, and 100 µm in diameter) and well-like invaginations (crypts, 120-170 µm in depth, and 50 µm in diameter) located between the villi. Cells proliferate in the crypts, and, as they migrate to reach the top of the villi, they differentiate into enterocytes[91].

The examples above illustrate the key role of the BM in determining the fate of epithelial cells, in the same manner as it is now widely established that cells respond to the mechanics[92], composition, topography and roughness[93] of their environment.

The basal lamina is also a site where the crosstalk between the epithelium and the mesenchyme takes place. Epithelial and mesenchymal stem cells interact via secretory signaling molecules, ECM and direct cell-cell junctions. Cells on each side of the BM influence the development of cells on the other (*e.g.* mesenchymal cells are implicated in the formation of the epithelium, and epithelial cells induce smooth muscle cell differentiation). These cell types work thus concomitantly to define tissue morphology during organogenesis, as well as to ensure tissue regeneration and homeostasis[94]. For instance, in urinary and GI tracts epithelium Sonic hedgehog (Shh) mediates smooth muscle cell differentiation and promotes mesenchymal cell proliferation. On the other side, in the mesenchyme, fibroblasts' growth factor 7 (FGF-7) stimulates the differentiation, proliferation and arrangement of epithelial cells at their early stage, while transcription growth factor 1 (TGF-β1) plays a role in cell differentiation[95,96]. Cells from the luminal layer provide growth regulatory signals for the underlying SMC[37]. For instance, Wei *et al.* revealed that the addition of epithelial cells on a scaffold enhances muscular regeneration[97], that depend on a biochemical cascade initiated by ECs. The release of lactate stimulates the promotion and the polarization of macrophages. Under their impulsion, myogenic progenitor cells (MPCs) activate to proliferate, differentiate and fuse into myofibers to restore the damaged muscle. ECs are thus a key player in muscle regeneration and revascularization[98] and their crosstalk with muscular cells should be fully considered in the development of the different cell types mentioned just above.

Basal membrane mediates epithelium formation and restoration through different biological and physical factors. However, its influence over the muscular layer has been poorly investigated. Although cellular behavior is probably guided by BM's physical (permeability and mechanics) and biological (growth factors and binding sites) properties, research has not been able to clarify this interdependence until now.

2.3 The muscular outer layer

In tissue engineering—and in particular when following a biomimetic approach to develop new materials—it is critical to reproduce the structural and compositional features of the targeted tissue. This is particularly relevant in the case of the muscular outer layer, since it is the first barrier against excessive expansion of the tubular tissues in cases where the luminal pressure increases, while the adventitia's role is mostly to prevent wall rupture. This layer is thus key for the biomechanical functions of tubular tissues. Structural fibrous proteins (collagens, elastin and laminin) as well as glycosaminoglycans (GAG) provide a robust skeleton to cells embedded in the matrix, mainly smooth muscle cells (SMC).

In arteries, the tunica media is a fibrous ECM layer mainly composed of type I collagen (ColI)[99](Table 1). In GI tract and esophagus, type III collagen is the main component of the mucosa, and forms a network that provides anchorage to smooth muscle cells[54]. In trachea, several types of collagen subtypes are involved and assume different roles, however 80 to 90 % of the total collagen moiety are represented

by type I, II and III collagens. Type II is the main component of airway cartilage and facilitates chondrogenesis, whereas type III and especially type I collagens provide the ECM with mechanical stability[100]. Finally, type I collagen dominates the composition of the muscular layer of the ureter, with 83 % of the global wall composition[101]. Considering the predominance of collagens in native tubular tissues and in particular in the thickest and outer muscular layer, their use as a raw material is essential to fabricate biomimetic tissues. Still, the accurate quantification of their content in healthy tissues, about 100 to 200 $mg.mL^{-1}$,[102], remains imprecise which raises major challenges to design consistent strategies for the elaboration of biomimetic tubular tissues grafts. This aspect is of particular importance due to the lyotropic behavior of collagen in solution and its impact on the fibrillar architectures obtained after fibrillogenesis[44]. If the concentration of ColI has not been established for many tissues, its organization within these tissues has been widely described in the literature over the past decades, as described in the introduction. Variations in the conformation of the collagen molecules and network modulate interactions with cells, and the cellular responses might vary with the number of exposed binding sites, tightness of the network and fiber sizes, among other factors. For instance, residual proteoglycans in collagen extracted from animal tissues is known to affect the antigenicity of the material[43]. Other studies showed that cell phenotype depends on the collagen conformation, in particular SMC that populate the muscular layer[103].

The SMC network is an active control system able to generate the contractile forces necessary to adapt the geometry and the mechanics upon physiological demands[69]. For example, in arteries, they respond to nervous and hormonal signals to modify the vessel volume and the blood pressure[72]. Their contraction is initiated by membrane depolarization, which activates voltage-gated calcium channels and leads to calcium (Ca^{2+}) influx into the cell, leading to its contraction[54]. Healthy contractile SMCs exhibit a spindle-shaped morphology, regulated by several signaling pathways and local environment cues[104]. Under certain conditions, for instance damaged tissue or *in vitro* culture, cells undergo phenotypic transitions that hamper the contractile behavior. Following the loss of their myofilaments, they flatten, lose their contractile function and become more proliferative. Regulation of their phenotype is a complex process that remains poorly understood due to its plasticity[105]. By identifying the conditions that favor one or another phenotype, these could be advantageously used to bioengineer tubular materials, generating phenotype-specific regions and guiding their reversibility. The composition of the tubular tubes could also be modulated to control the cellular behavior. On the one hand, it is known that fibronectin[106], monomeric type I collagen[26], or growth factors could promote the migration and proliferation in order to maximize the repopulation of the inner part of the material. Various growth factors are also known to favor SMC migration (transforming growth factor-β1 TGF-β1), proliferation (fibroblast growth factor bFGF), or both (platelet-derived growth factor PDGF)[74]. On the other hand, once SMCs are distributed in the material, favoring their subsequent transition into contractile SMCs could be achieved using laminin, elastin, heparin[106], hyaluronic acid (HA)[107], while fibrillar type I and

IV collagens at high concentrations would enable to reconstitute the adventice[108,30]. This complex approach requires a fine control over the material composition, and no example of such system was found in the current literature.

SMCs are not only impacted by the surrounding layers, but also by their local environment, the topography and porosity of the substrate. While tailoring the external surface using coatings or textural motifs enhance the epithelial cell adhesion[109], for SMC the limiting factors reside more in the penetration into the material with sustainable access to nutrients[55]. Porosity is the most important feature to increase viability and proliferation rate in a non-vascularized biomaterial, but in the meantime, increased porosity can compromise mechanical properties. Well-balanced pore characteristics—enabling both cell migration, proliferation, nutrients diffusion as well as the maintenance of the structural stability—need to be found for each targeted tissue.

2.4 Recapitulating tubular tissues layers

Research efforts to fabricate tubular tissue grafts have focused on a large panel of techniques and compositions, ranging from synthetic up to cell-derived compounds. Although the design of grafts has progressively approached the characteristics of native tissues, they still fail in demonstrating the physiological properties that should derive from biomimetic structure and composition. Some of these characteristics have become clear guidelines to rebuild environments favorable to cell migration, proliferation, and to provide accurate mechanical support. A general overview of such guidelines is presented in **Table 2** for each layer of the tubular tissues, dictated by their biological and mechanical properties summarized in Table 1.

As previously introduced in section 2.3, smooth muscle cells require access to the inner volume of the implanted material, as well as to nutrients to proliferate. In the absence of vascularization, these requirements can only be met by adjusting the porosity of the material. Size, shape and interconnectivity of the porous network determine cells migration kinetics. Parisi *et al.* compared the migration mechanisms of normal human dermal fibroblasts on a porous type I collagen matrix and an equivalent non-porous matrix. After 28 days, cells seeded on the porous matrix reached 6 times the depth through the material as compared to non-porous matrix (respectively ~700 µm and 110 µm from the seeding surface)[110]. A variety of methods allowing to modulate cell colonization is reported in section 3.2.2 of this review. One particularly important point in this context concerns the maintenance or induction of cell contractile phenotype which determine the materials' functionality but also could entail their loss of dimensional stability.

Table 2. Biological and physical properties of the tubular tissue structural layers.

Layer	Structure	Composition	Functions
Epithelial inner layer	Layer of cells lining the luminal surface of the organ, *i.e.* the interfacial basal membrane (BM). The latter is a two-layered structure composed of the *basal lamina* and the *lamina reticulata*.	Tissue-specific epithelial cells tightly bound together to form the epithelium. In the BM, collagen IV and laminin isoforms predominate in a fibrillar network along with entactin, perlecan, fibrinogen and fibrin.	To control permeation of the different components of biological fluids between the luminal space and surrounding tissue. Exchanges with the fluids (air, mucus, blood) and evacuation of eventual contaminants. The BM brings mechanical support, signaling functions for epithelium anchorage, and acts equally as a selective barrier allowing exchanges between the epithelial and muscular layers.
Muscular outer layer	Porous fibrillar network, divided into two to three layers in tubular tissues.	Smooth muscle cells embedded in a protein macroporous matrix, dominated by type I collagen and elastin.	Responsible for the mechanical properties and structural integrity of tissues. Hosts the SMC network able to generate the contractile forces.

The processes involved in epithelium formation relies on diverse cell locomotion modes (collective, mesenchymal, amoeboid) that are regulated by textural, mechanical and biological cues. In this regard, the texture of the luminal surface should promote cell adhesion and minimize cell infiltration, suggesting that porosity—at the length scale of the cell—should be minimized. Textural motifs might facilitate adhesion and proliferation of cells[111]. Fabrication routes based on the coating of the luminal surface with proteins from the basement membrane (collagen IV and laminin isoforms) should allow reproduction of the complex biological cues that favor cell anchorage and subsequent epithelialization. Beyond biological cues, such an approach should cover and smoothen the luminal surface and thus minimize cell infiltration.

Numerous studies have shown that collagen is an ideal substrate to develop 3D biomimetic matrices[43,112]. Because type I collagen behaves as a lyotrope in solution, there is a strong link between its concentration and the formation of liquid crystal mesophases. Upon fibrillogenesis, these structures lead to a variety of suprafibrillar architectures that are crucial to understand the relationship between the graft and its

environment, but also to achieve functional graft materials. Control over the collagen concentration in the physiological range, coupled to the ability to tailor its textural properties remain ultimate goals to the research community dealing with collagen-based biomaterials', and more generally with biomimetic approaches to the elaboration of functional grafts in tissue engineering. The following section discusses the strategies—their forces and their shortcomings—to tackle this goal

3. Biomimetic strategies to recapitulate tubular tissue layers

3.1 The epithelial inner layer

3.1.1 Challenges of epithelium replacement

The absence of epithelium, both in pathological tissues or in grafts currently used in clinical practice, is one of the major causes for tissue or graft failure. Such limitation results in bacterial colonization, occlusion of the construct or tissue, or leakage[81]. A focus on the reconstruction of this layer is thus crucial for the proper function of tubular tissues. One strategy to favor the generation of epithelia relies on *in situ* grafting of the epithelial layer harvested from an analogous tissue. Currently, buccal mucosa grafts are the most common substitutes in urology, with a success rate of 70 to 80 %[113]. However, autologous transplants of epithelial grafts are often associated with donor-site morbidity, slow dedifferentiation to match the host tissue epithelium, functional misfits (stenosis, fibrosis, and contraction[114]) as well as deleterious side effects at the harvesting site for patients. These procedures significantly reduce the quality of life of patients. Buccal mucosa harvesting, for instance, induces pain, bleeding, difficulties to swallow, reduced mouth movement (opening, smiling, whistling, speaking), as well as profound impact on of salivation, taste and diet[113]. Both the harvesting procedure of autologous transplant and the implantation procedure are challenging. Implanting epithelia harvested from a different tissue might also lead to undesired physiological features if cells are not able to dedifferentiate. It is often the case for oral mucosa replacement using skin grafts, associated with excessive mucus formation and more surprisingly, hair growth[115]. The inability of these advanced surgical grafting techniques to restore the physiological functions together with the non-negligible side effects both challenge the biomaterial community to develop new solutions for epithelization. The alternatives proposed by the tissue engineering community tend to reconstitute the native basal membrane, with simplified structure/composition. These approaches result in lesser specificity towards certain cell types, decreased number of anchoring sites and signaling functions. The following sub-sections address the current and future strategies to promote epithelium reformation, illustrated in **Figure 3**.

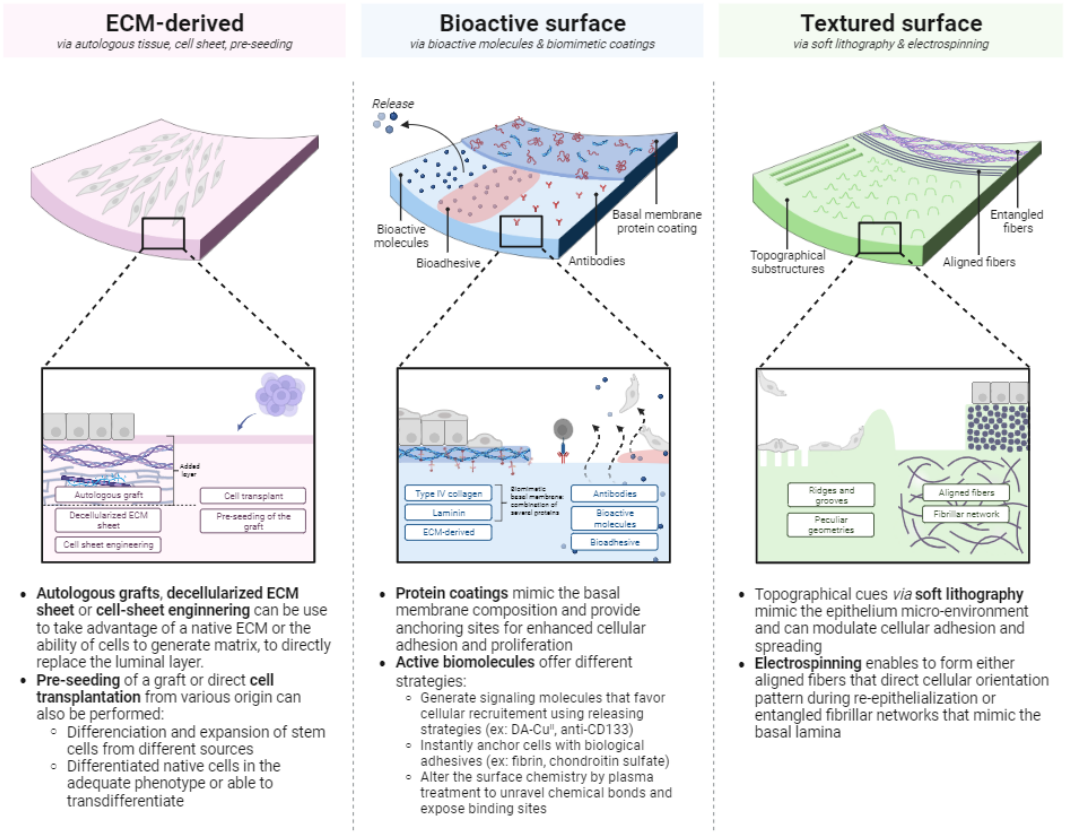

Fig. 3. Tubular tissue epithelium recapitulation. Strategies can be reduced to three main pathways: (a) ECM-derived epithelial layers, (b) bioactive surfaces and (c) textured surfaces.

3.1.2 Pre-seeding

A strategy for scaffolds unable to be quickly repopulated by cells, is to restore the epithelial layer by direct *in vitro* cell seeding prior to the graft implementation (**Fig.3**-ECM derived). The issue that dominates this approach is the reliability of the cell source. Collecting either autologous or allogenous cells able to differentiate is a difficult process, further adhesion on the scaffold is stochastic, and maintaining their phenotype and regeneration abilities require to provide the adequate environment. If cells are not able to do so, it results in graft rejection[116]. Additionally, due to the use of living cells, autologous tissue engineered products are subject to a severe regulatory framework that restrains the translation from the laboratory to the clinic[117].

Urothelium repair is currently the easiest and the most standardized epithelium replacement procedure. A new procedure was established for its repair in 2015, inspired by the conventionally used oral mucosa tissue for which a small number of autologous cells are expanded to form a cell sheet, later implanted for anterior urethroplasty[118]. The material, named MukoCell® is used for urethral stricture surgery with an efficiency of 84% treated patients, and is one of the few tissue-engineered products available in the

European market. Replacement of the urothelium in urinary tracts is a minor field of research in biomaterials and cell therapy, but pre-seeding techniques for the bladder replacement have been extensively studied. Because these tissues share the same urothelium it is likely that the methods developed for the bladder may be transposed to the epithelization of urinary tract. With a similar phenotype to mesenchymal stroma cells, urine-derived stem cells (USCs) can be reprogrammed into iPSCs[119]. Under appropriate cell culture conditions, it is possible to induce the differentiation of human iPSCs into bladder-associated cell types, including urothelial, endothelial and smooth muscle cell-like lineages[120], overcoming cell sourcing issues[113,120,121]. The potential of alternative sources like human bone marrow mesenchymal stem cells have also been studied to induce the simultaneous differentiation of both SMCs and UCs under appropriate culture conditions[122]. Urothelium bladder engineering currently relies on several sources of stem cells which enable relevant differentiation and proliferation *in vivo*[122]. The formation of a mature stratified bladder urothelium was shown by Suzuki *et al*. via a high primary dose administration of an inhibitor of the GSK-3 enzyme, implicated in inflammation and cancer cell proliferation[123,124]. But so far, only one study was able to demonstrate the reformation of an urothelium *in vivo* following cell transplantation. This first successful transplant of UC into the bladder lumen was performed in 2019[124]. UCs were transdifferentiated from human dermal fibroblasts using four transcriptional factors (FOXA1, TP63, MYCL and KLF4) that are expressed *in vivo* during urothelium formation and support mesenchymal-to-epithelial transition. After only 4 days of *in vitro* culture of the transdifferentiated fibroblasts, the transplantation into the bladder of a mice with damaged urothelium was performed and induced the conversion of the fibroblasts into UCs in the native environment. Overall, transplantation of cells is a possible and effective pathway for urothelium reformation, which allows variations in the cell source and transplantation method.

Regarding other tubular tissues, procedures are still experimental and no gold standard has been established. Airway epithelium reconstruction is limited by the difficulties of culturing primary human respiratory epithelial cells and maintaining their phenotype[116], partly due to the lack of mechanical resistance of the scaffold in the absence of cartilage. Attempts of replacement by autologous nasal squamous epithelium showed that the luminal epithelial surface can be recovered following transplantation[125,126]. Combined to the cell sheet method introduced by Kanzaki *et al.*[127] on pre-vascularized bioartifical grafts, Dang *et al.* developed sheets from those cells and incorporated them in partially decellularized grafts to improve re-epithelialization[126]. Noteworthy, they succeeded in preserving viable cartilage cellular components able to gradually restore the luminal architecture that still prevent immune rejection. While in most cases decellularization of trachea fail to retain cartilaginous components, impeding the restoration of the structural and mechanical properties that prevents luminal collapse. For the cell sheets, nasal epithelial cells were harvested in rabbits and expanded onto type I collagen-coated petri dish. At confluence, cells were seeded on thiol-modified HA-PET insert, and after three weeks, cell sheets were detached and harvested. The method enables to

generate a multilayered mucosal epithelial structure with the characteristics features of airway epithelium, *i.e.* tight intercellular junctions, rounded morphology of the cells and low expression of anti-vimentin antibodies. Autograft transplantation in rabbit model following tracheal partial resection demonstrate the rehabilitation of the tracheal functions after 2 months, with a thin tracheal wall devoid of fibroproliferation, stenosis and granulation, displaying a lustrous and smoother appearance.

Esophagus epithelium replacement by cell therapy is still poorly investigated, and if so, mostly by pediatric surgeons. From the few articles available in the literature on this topic, the same strategies used for urothelium reconstruction prevail: either a generation of cell sheets further inserted in the scaffold lumen[128], or the seeding of autologous cells[129]. Differently from the previous approach, Saxena *et al.* studied the insertion of epithelial cell sheets onto a biomaterial rather than a decellularized matrix[113]. Epithelial cells were harvested in rat esophagus and transferred onto OptiMaix-3D®, a porous collagen matrix fabricated via solidification and freeze-drying of 1.5 wt% of collagen (mainly ColI) and elastin, previously sewed into a tube and pre-coated with 25 mg/mL ColI. After 8 weeks *in vitro*, cells exhibited the characteristics of mature epithelium (CK-14 markers) and formed a continuous layer on the lumen. Similar to the urothelium, both differentiated native epithelial cells and stem cells were studied and the two cell lineages were able to adhere on the substrate, proliferate and maintain or differentiate into the appropriate phenotype to reconstitute a mature epithelium[129].

The gastro-intestinal epithelium possesses outstanding regeneration abilities, with the fastest renewability. Formation of the crypt-villus units—epithelium included—is a self-organized process, able to originate from a single stem cell[130]. In homeostatic conditions, renewal is initiated by the transcription factors of the quiescent reserve stem cells in the crypts, the *leucine-rich repeat-containing G-protein coupled receptor 5*-stem cells (Lgr5+). Their proliferation leads to the spontaneous formation of multicellular 3D clusters named organoids. *In vivo*, new cells arise from these organoids, which proliferate and differentiate while migrating towards the crypt-villus axis[131]. Organoids also provide specific intestinal luminal cells, such as goblet and enteroendocrine cells, as well as mitotic cells[132]. Expanded *in vitro*, Lgr5+ cells produce organoids able to self-organize into an epithelial microvilli architecture with complex junctions, similar to what is observed in histology section of native tissues. The high potential of Lgr5+ to retain self-renewal properties and the ability to form organoids to repair damaged epithelium *in vivo* was confirmed for the first time in 2018, with a successful transplant of human colon organoids onto mice[133].

To the best of our knowledge, no cell transplant from autologous or stem cells were developed for the circulatory system. However, cell sheet engineering has been extensively studied to build either the luminal layer or the complete biomaterial for vascular applications[36].

Overall, two cell-based strategies enable to restore the epithelial layer of tubular tissues. Cell deposition on scaffolds or directly on the injured site can be conducted using either differentiated cells or stem cells. Cells might originate from another epithelial tissue (for instance, the oral mucosa EC for the urothelium) or from other individuals (for instance, human organoids onto mice intestine). However, it requires a control over the kinetics of the proliferation and the appropriate phenotype induction. The insertion of cell sheets grown *in vitro* into decellularized matrices or into engineered scaffolds allows to provide a more complex composition to the luminal surface. Production of ECM components by cells increases the repairing kinetics and favors biointegration which results in increased mechanical stability of the tubular organs.

3.1.3 In vivo recruitment of cells through active coatings

Another approach to reconstitute the epithelium is to design a luminal environment that actively induces epithelial cell migration[81] (**Fig.3**-bioactive surface). *In vivo* epithelialization requires a control over the cell migration (textured surface, signaling pathways and native environment) and the interactions with the surrounding cells (smooth muscle cells and mesenchymal stem cells). In particular, controlling the speed of cell migration *in vivo* is pivotal to ensure the coverage of the luminal surface, and avoid any clinical issues arising from epithelia depletion. To do so, many strategies attempt to mimic the basal membrane by topographical patterns or local supply of substances to endow the scaffold with high epithelialization ability and SMC phenotype regulation[37,81,91,134,135]. Wrinkled surfaces in the intima layer favor adhesion, oriented growth and phenotype differentiation of cells[91]. Approaches based on the integration of signaling molecules in the composition of the substrate are more reliable, but regulation of their release kinetics remain challenging[91].

Active biochemical coatings to regulate cell adhesion

Recent strategies have demonstrated an increasing potential of using active biomolecules to promote epithelialization. A simple and efficient approach relies on the decoration of the surface of the tubular grafts with antibodies onto which cells' antigens bind. CD133 antibodies are a good example for their ability to promote adhesion of circulating hematopoietic and endothelial regenerating cells presenting CD133 antigen glycoprotein on their surface. Encapsulation of antibodies has been studied in porous scaffolds by Wu *et al.*[136]. The core/shell electrospun scaffold presented a porous yet mechanically resistant outer layer composed of poly(L-lactide-co-caprolactone) (PLCL) and type I collagen (ColI), and a smooth inner layer of PLCL/ColI nanofibers/Heparin. The encapsulated antibodies were efficiently released, and a significant increase in the recruitment of endothelial cells *in vitro* was observed compared to the control without antibodies. Further *in vivo* investigations in rat abdominal aorta for 2 months confirmed the inhibition of coagulation by Heparin in the early period of implantation, and the promotion of EPCs recruitment and maturation on the luminal surface.

Aside from antibodies, ions or biologically-derived molecules have been equally investigated. Wang *et al.* established that the addition of dopamine-mediated copper(II) ion (DA-Cu^{II}) system on electrospun films significantly modulate the cell fate of ECs and SMCs and the platelet adhesion via a catalytic production of (NO) *in situ*[91]. In contrast to the control —without Cu^{2+} ions—NO was generated over a long-term period, less platelets adhered, and no blood clot was formed. *In vivo* evaluation performed on rat abdominal aorta model demonstrated a high patency rate for DA-Cu^{II} of 66.7 % after 3 months whereas all controls were occluded after 15 days.

Addition of active complexes as DA-Cu^{II} and CD133 in the scaffold enables to modulate biological signaling in favor of epithelial cells' recruitment. Integrating these molecules into a bioadhesive layer yields even higher cellular adhesion rates. However, the challenge of maintaining the adhesive strength within the moist environment of native tissues remains to address. Bioadhesion is a mechanism spanning the whole animal kingdom (gecko, frogs, mussels, among others)[137] that constitute an inspiration for its potential to influence (bio)materials science research. Numeros examples of applications are available, ranging from wound healing (sealants and hemostatic agents[138]) to surgical tools for specific treatments[139]. In the case of grafts, marine mussel byssal plaques have provided inspiration for enhanced adhesion thanks to their high proportion in 3,4-dihydroxyphenylalanine (DPA). The adhesive system, composed of electrostatically self-assembled lysine and DPA-functionalized poly(acrylic acid) (PAADPA), was studied as a new adhesive coating strategy to prevent restenosis in injured arteries[140]. *In vivo* assays revealed increasing presence of endothelial marker CD31 on cells at the neointimal surface from day 3 to 7 and 14, alongside with a thick epithelium reformation.

Altering the surface biochemistry of biomaterials by plasma treatment has also been recognized as an efficient pathway to enhance protein absorption, by tailoring the surface with carboxyl groups, immobilizing biomolecules such as ECM proteins, improving biocompatibility of porous surfaces and changing hydro- or oleo-phobic properties. This technique has produces interesting results for synthetic polymers, but its translation to biopolymers has not been reported yet and requires further research efforts[141].

Protein coatings to enhance epithelization

Using one or several components of the BM to line the luminal surface of biomaterials favors epithelial cell adhesion, biocompatibility and impermeability by providing native anchoring sites[134]. Biomaterials obtained from decellularized ECMs, can be efficiently used as a coating since they retain the macro- and micro-architecture of the original native tissue, as well as their complex composition (**Fig.3**-bioactive surface). Fayon *et al*. studied the coating of human decellularized Wharton's Jelly—mainly composed of type I collagen—on an arterial substrate[135]. Seven days after EC seeding, the material

showed good hemocompatibility and a density of cells 3 times higher than the control, a non-coated ECM-derived material. The complex biological composition combined to the native conformation of the components offered by the decellularized ECM coating efficiently improved the endothelialization. However, the technique remains far from being translated into clinical settings, since it relies on tissue banks, it requires facilities to perform cell culture and there because concerns over compatibility persist[135]. Single proteins extracted from mammalian ECM are already available on the market and constitute an interesting alternative. However, native proteins from mammalian ECM remains a relatively marginal strategy in the field of research dealing with biomaterials' coatings. The zoology of these proteins includes laminin (Ln), fibronectin (Fn), heparin (Hep) and type III and IV collagen (ColII, ColIV). Opposite to ColI, ColIII is not thrombogenic because it lacks the sites for platelets, while it still favors the adhesion of ECs. Hence its use as a coating on a scaffold, either synthetic or biologically-based, effectively promotes re-endothelialization[34]. Similarly, hyaluronic acid (HA), a polysaccharide, is widely used to prevent coagulation that contributes to hinder luminal re-endothelialization[142]. This trend is supported by Luo *et al.*, who used materials patterned with HA to study the synergic effects of several BM protein coatings[134]. Ln coating and co-deposition of Ln and ColIV demonstrate the lowest platelet adhesion and activation, along with enhanced proliferation rate for both ECs and SMCs. For SMCs, the contractile phenotype was maintained, further inhibiting hyperplasia, whereas the control—a non-coated surface—induced a shift toward a flat phenotype. Cytocompatibility studies demonstrated the ability of Ln and Ln+ColIV to promote the release of NO, inhibit the adhesion of macrophages while maintaining their anti-inflammatory phenotype (M2), which was further confirmed by *in vivo* studies. After 1-month dorsal sub-cutaneous implantation in rat models, substrates with coatings exhibited lower inflammatory response, with a fibrous encapsulation layer 2 times thinner than the control. What emerges here is that the use of a protein coating with a single component favors the endothelialization process, but the combination of several proteins mimicking the BM enhances its efficiency and boosts the proliferation of both ECs and SMCs. The remaining challenge of coatings is their application to tubular tissues, in particular in terms of their homogeneous application and controlled position at the lumen of the constructs.

3.1.4 Patterned luminal architectures to guide cellular behavior

Soft lithography

Contact guidance[143] induced by microtopography is based on a controlled arrangement of fibers or textural motifs (grooves and ridges) to guide and orient cells[109,149]. While the technique has mostly been applied to elaborate microfluidic devices, soft lithography can be transposed to larger biomimetic tissues with the purpose of promoting contact guidance (**Fig.3**-textured surface). This technique is particularly adapted for peculiar geometries such as those of the gut, featuring crypt and villi structures. Wang *et al.*

used it to form thin membranes of type I collagen at 5 mg.mL^{-1} from a PDMS mold with micro-well arrays[68]. *In vitro* assays resulted in surprising conclusions: a biomimetic topography is not necessarily required for intestinal epithelium reformation. Reproducing the depth of the crypt structures found in native tissues led to confinement of an intestinal epithelial cell line (Caco-2) and poor cell-cell interactions with delay in spreading and inhibition of their differentiation.

The difficulty to translate the soft lithography from planar to tubular geometry was overcome for the first time in 2016 with a synthetic polymer[144]. Topographical niches of 2 mm were created by thermal-based nanoimprint lithography method on tubular PDMS molds. These were dipcasted several times in poly(vinylalcohol) (PVA) cross-linked solution and dried to obtain the final scaffolds. Implantation in infrarenal aorta of rats demonstrated that patterned surfaces induce self-endothelialization and no patency, in comparison to unpatterned grafts that were occluded after 20 days. Use of soft lithography techniques in biomaterials research remains scarce, but the results suggest that this easy and effective route to guide cell fate deserves more attention from the community.

Electrospun fibers

Electrospinning is a widespread method to create porous biomaterials, with tunable properties such as the polymer composition, number of layers, their thickness, the fibers' diameter and orientation. These parameters result in a diversity of materials with variable porous network. Generally, the system is composed of a polymer dissolved in a volatile solvent dispensed through a needle, a high voltage source and a target. Polymer is electrically charged and extruded into thin threads through the needle, and collected on the target thanks to their potential difference. The obtained polymer meshes exhibit fiber diameters ranging from nm to µm in dry state, since the solvent evaporates during the process[145]. The use of synthetic polymers still dominates the field, but a few biopolymers have been processed by electrospinning, including chitosan, native and degraded type I collagen (gelatin)[146], or biodegradable polymers such as polycaprolactone (PCL) and polylactic acid (PLA). They efficiently promote cell adhesion[147] by providing biochemical cues similar to the ECM. The versatility of electrospinning can generate entangled protein networks that mimic the native BM by co-electrospinning several biopolymers to obtain core-shell structures or by the creation of double-layered structures by successive electrospinning of different components or by patterning techniques[148,149]. Biological materials such as decellularized ECM (dECM) of bovine aorta can be incorporated into a polymeric solution and electrospun to form tubular constructs. This combination is beneficial to mechanical properties with the use of the polymer and to cell adhesion and proliferation through increased hydrophilicity by the dECM[150]. Electrospinning also permits to align fibers that guide cell growth, positively affecting spreading, differentiation and formation of typical elongated epithelial patterns[151]. Orientation of the

fibers in aligned wrinkled patterns similar to the arterial lumen can orient endothelial cells growth while limiting platelet adherence and activation[91]. PLA/silk fibroin (1:1) scaffolds with longitudinally oriented nanofibers enabled the formation of a dense layer of HUVEC after 5 days of culture, with a spindle shape morphology parallel to the motif's axis. The resulting material can encapsulate signaling molecules and gradually release them to promote cell adhesion and proliferation[91,149], however, the intrinsically porous structure cannot avoid cell infiltration within the scaffold wall, hindering epithelium reformation. Reduced porosity specifically on the luminal surface can be engineered by adjusting the process parameters (polymer concentration, speed, distance to the mandrel and voltage). Porosity can be modified by additional post-processing steps, for instance by the addition of a supplementary coating, with the dual advantage of filling the pores and exposing a higher number of binding sites for ECs adhesion. Many examples in the literature feature an outer porous layer of PCL, HA or PLA combined to a smoother inner layer integrating collagen or derived components (gelatin[146,152] and recombinant human collagen[108]. In most cases, collagen is electrospun with other polymers or crosslinked in a second step to preserve the shape and porosity. Both conditions preclude collagen self-assembly into fibrillar structures, hindering the formation of the characteristic structures found in native tissues. Moreover, crosslinking steps require the use of harsh chemicals (genipin or carbodiimides) that can be detrimental to cell survival. Dems *et al* demonstrated for the first time that pure collagen could be electrospun without any cross-linker, by replacing the crosslinking step with an ammonia-rich atmosphere to induce self-assembly. The resulting self-standing flat membrane exhibited the typical characteristics of collagen fibrils found in tissues, *i.e*. the D-banding pattern observed under TEM corresponding to native collagen fibrils and a bi-refringent signal under cross-polarizers demonstrating the existence of liquid-crystal like motifs[153]. Briefly, collagen was dissolved in a mixture of hydrochloric acid (3 mM HCl, pH 2.5) and ethanol (75 %vol) with a final concentration of 1.7 $mg.mL^{-1}$. Solvent was evaporated overnight at room temperature, and fibrillogenesis of the collagen molecules was performed in ammonia vapor for 20 minutes. Samples were rinsed in culture medium 3x/day for 10 days to remove all ammonia residues, before cellularization. Long-term cytotoxicity assay performed with normal human dermal fibroblasts showed that the membrane promotes cell spreading with clear stress fibers distribution in the cellular body and spindle-like shape morphology. Further investigations are needed to clarify if these interactions are equally found in epithelial cells and thus if electrospun collagen could be used to line the inner part of a tubular biomaterial.

The examples mentioned above illustrate the relevance of electrospinning as a cost-effective and scalable process to reconstitute partial organ structures from entangled fibers, able to influence cell movement, proliferation and phenotype by topographical and compositional cues. Although the field is relatively new, we anticipate that electrospun materials composed of biomolecules from the ECM will play an increasingly relevant role in the development of functional tubular tissues.

3.1.5 Advantages & disadvantages of each technique

We discussed above a selection of fabrication methods able to reproduce the luminal layer of tubular tissues, with a focus on biomimetic approaches, and how they succeed in promoting epithelium reformation. Three major pathways and types of surfaces stand out: (a) ECM-derived (b) bioactive and (c) textured, as illustrated in Figure 3. Additionally, we compared in detail the methodologies within these 3 categories to provide guidance in their elaboration and present the key challenges that still need to be addressed (Table 3).

Table 3. Comparison of various methods for biomimetic tubular tissue epithelial layer elaboration. Advantages and disadvantages as well as key literature references are given for guidance in fabrication.

Approach	Method	Advantages	Disadvantages	Key references				
				Vascular	Trachea	GI tracts	Esophagus	Urinary tracts
ECM-based surfaces	Autologous grafts or allografts	Native structure and composition.	The harvest might be harmful to patients. Its implantation is associated with biocompatibility issues, undesired physiological features (ex: hair growth on the oral mucosa), or availability dependency to tissue banks.	[36]	[116]	N/A	N/A	86, 87 All references in this section were previously gathered by Ławkowska *et al* in 2023[113]. To our knowledge, there is no tissue engineering approaches at the clinical level specifically targetting the urothelium of ureter.
	Pre-seeding	Reconstitution of a mature and permeable epithelium displaying the typical	Long procedures that requires a relevant cell source. Difficult to	N/A	[125–127,154]	[130,132,133,155]	[128,129]	[156] References for the bladder, which possess the same

		immunohistological characteristics. Possibility to vary the cell source, either specific to tissues or undifferentiated.	implement in clinical context.					urothelium as urinary tract: [120–124,157]
Bioactive surfaces	Active biomolecules	Simple procedure to promote cell recruitment through the addition of signaling molecules. Treatment of the surface by plasma enhances cell adhesion.	Requires a precise control over the releasing kinetics and identifying the ideal cell seeding concentration. Plasma treatment is difficult to apply at the luminal surface and has not been translated to biopolymer-based tubular materials yet.	[140]	28,91	N/A	N/A	N/A
	Biomimetic protein coatings	Efficiently promote cellular adhesion and proliferation by a single protein coating. Possibility to combine several proteins for enhanced adhesion.	Difficulty to deposit a coating on tubular structures and ensure its maintenance to endure the physiological functions (flow and mechanical stress).	N/A	19,28,89–91,93,95	28,50	N/A	N/A

Textured surface	Soft lithography	Straightforward method to create and tailor geometrical patterns.	Surprisingly the biomimetic topography is not necessarily an advantage in the epithelium reformation, in particular for intestine. If the designed wells follow the native architecture, cells are confined and cannot restore junctions but such behavior could be related to the composition of the materials that can be processed by soft lithography.	144,150	N/A	68,158	N/A	N/A
	Electrospinning	Easily scalable, possibility to create an entanglement of several components to mimic the BM. Provides a porous network compatible with drug eluting systems.	The porous network can induce cell migration into the scaffold, hence limiting the epithelium formation kinetics. The technique requires biopolymers that can be electrospun.	152,153	147,151,153	91,153	151	146,149,153

3.2 The muscular outer layer

Research in the field of tubular organs' replacement revolves around bioengineering approaches to recreate the muscular layer. This requirement is often complemented by an engineered epithelial layer using the strategies described above. A large array of techniques has been explored to develop scaffolds with adequate structural and compositional features, which are commonly divided into two main approaches: acellular or cellularized scaffolds. Cellularized scaffolds have the benefit of proposing "ready-to-use" materials, simplifying its application. Moreover, they can be considered as platforms to understand cell-material interactions and to study the materials' potential biointegration.

However, they raise multiple issues regarding cell viability during processing, host cells compatibility and sourcing[159], and custody from fabrication to implantation. Although a few pre-cellularized muscular layer models will be cited, this section will mostly focus on acellular scaffolds, in particular since these impose far less logistics hurdles. Acellular scaffolds rely on the assumption that the material will be repopulated by the cells of the host following implantation, either by means of a *porous* material facilitating cell migration, or via a *dense* material promoting cell adhesion and followed by material remodeling. The challenge of designing successful acellular porous scaffolds is to combine a porous network to promote cell migration, while achieving the required mechanical properties to restore the physiological functions. Dense materials offer a more complex composition, closer to native tissues, often integrating biologically-derived components such as cells, organoids or materials generated by cells[160]. The following sections aim at classifying the array of available manufacturing methods (advantages, disadvantages and challenges) to reproduce the muscular layer, illustrated in **Figure 4** and **Table 4.**

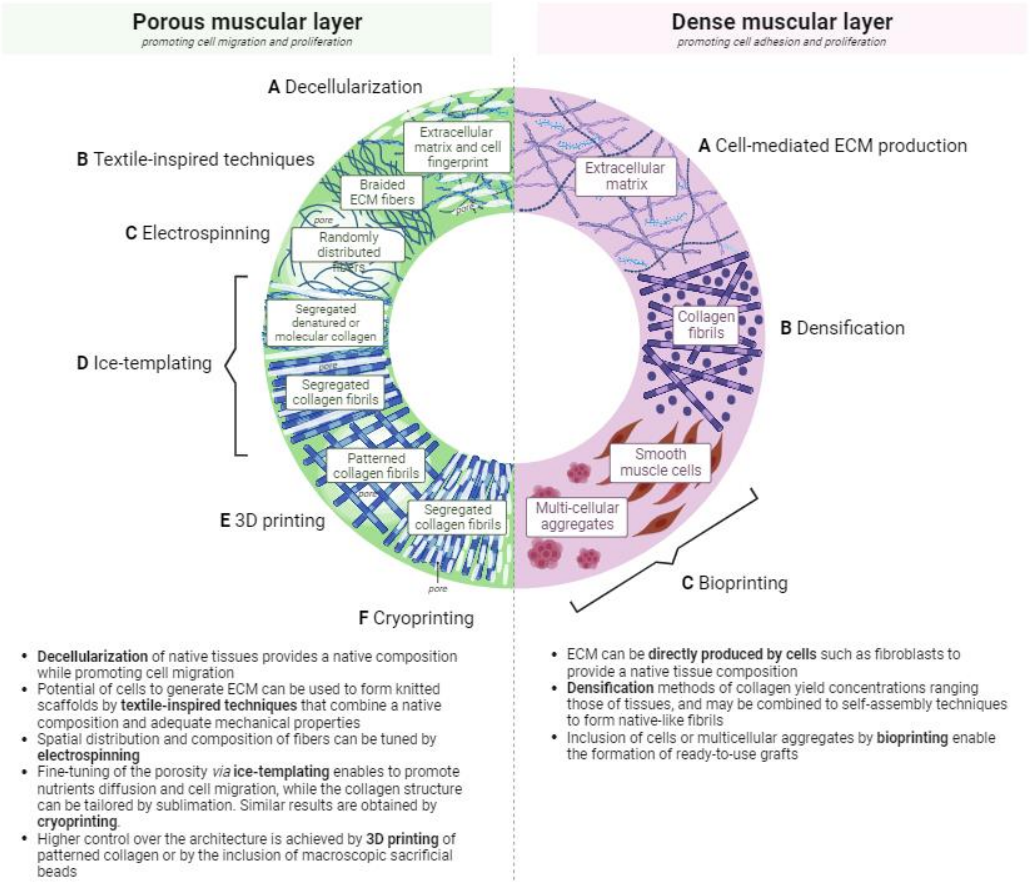

Fig. 4. Tubular tissue muscular layer recapitulation. Biomaterials can be reduced to two main pathways: *Porous* or *Dense*. Six techniques allow to generate porosity to promote cell migration including (**A**) decellularization, (**B**) textile-inspired techniques (**C**) electrospinning, (**D**) ice-templating, (**E**) 3D printing, and (**F**) cryoprinting. Three techniques allow to generate dense materials from biologically-derived components to favor cell adhesion and remodeling including (**A**) cell-mediated ECM production, (**B**) densification and (**C**) bioprinting.

3.2.1 Promoting biointegration with acellular porous materials

Decellularized ECM providing a native composition

As discussed in the introduction, decellularization process enables to remove cellular components from a tissue, while preserving its micro and nano-structure, complex composition and eventually its mechanical properties[160]. Beyond mature tissues, embryonic and fetal-derived tissues may also be used for their ability to foster regeneration[161]. Decellularized chorion membrane shows encouraging results in arterial tissue regeneration[162]. Wrapping the decellularized chorion membrane into a tubular structure provides mechanical properties in the range of the saphenous vein and promotes ECs proliferation on the lumen. However, the exact reasons behind successful replacement using a certain type of decellularized tissue remain unknown. A striking example is allogenic decellularized trachea, which fails to replace itself whereas cryopreserved aortic allografts allow for complex tracheal and bronchial reconstruction[163]. Briefly, human cryopreserved (-80°C) aortic allografts are mounted on custom-made

stents to prevent collapse, and transplanted into patients with severe cancers. Radical resections of the lesions were performed prior to implantation. The clinical study has been running for a few years, with now 44 patients treated with that technique. Other attempts of translational transplant have been done in arterial surgery using decellularized small intestinal submucosa (SIS), based on its high content in type I collagen (90 %). The local treatment of injured vascular tissues with SIS patches is efficient and shows good neovascularization and host cells infiltration[164]. However, if applied to larger structures such as a complete esophagus or an artery, it may lead to stenosis or thrombosis due to the loss of components during the decellularization process or to the thrombogenic effect of collagen in direct contact with blood[165]. To overcome the risk of blood clotting it is possible to seed endothelial cells at the luminal surface of the tubes to restore the physical separation between collagen and blood and thus avoid platelet adhesion[166]. To replace other tubular tissues, however, decellularized SIS matrices play an increasingly important role[39]. Pig-derived decellularized SIS has been tested for the reconstruction of the urethra of two patients. The follow up showed a continuous re-formation of the mucosa while the implants were progressively degraded. Post-operative assessment by intravenous urography at 12 months showed no anastomotic stenoses along the ureters[167].

Another strategy to favor the use of decellularized matrices in the context of tubular tissues' grafts relies on their application in presence of a stent. The use of stents reinforces the mechanical stability of the decellularized matrices and allows time for epithelial and muscular migration onto the cell-free scaffolds[168]. In this context the timing of stent removal has a strong impact on the scaffold cellularization and, more generally on clinical course after implantation[169].

Overall, using decellularized matrices offers suitable alternatives for a few tissues, providing native architecture and composition. However, the process involves high costs, may require several surgeries, and as for any biologically-derived tissue it raises standardization and industrialization issues[170]. Still, improvements of the regeneration process offer great perspectives. Optimization of the decellularization protocols to reach higher architecture and composition preservation rates is currently an active field of research with different techniques emerging rapidly[39]. The reduction of the number and the concentration of the chemical agents used for decellularization and the combination of physical and chemical treatments are the leading research avenues[24,168,171]. It would allow to extend the technique to more tissues, as urinary and GI tracts. Beyond the example mentioned above, urinary tubes are poorly studied despite the existence of extensive studies on the bladder—that holds comparable wall composition and architecture[172,173]. One of the most exciting challenges in the domain is to preserve intact villi in decellularized GI tracts, precluding the possibility for self-replacement. However, to the best of our knowledge, no reports have described the preparation of such a decellularized matrix[161].

Textile-inspired techniques

The use of textile-inspired techniques to mimic the architecture of native tubular tissues has attracted increased attention in the past decade. Zhang *et al.* proposed a fully reconstituted vessel, by combining electrospinning and braiding techniques[174]. Materials prepared from sequentially electrospinning silk fibroin (SF) and poly(L-lactide-co-ε-caprolactone) (PLCL) with a ratio of 30/70 were used to replicate the intima, while higher ratios of SF of 50/50 or 70/30 conveyed higher stiffness to replicate the media. The outer layer of the materials was composed of a braided silk fibroin structure to prevent wall rupture and to favor cell migration within the large spaces left between the yarns. The overall construct shows higher mechanical properties than native tissues, exhibiting a tensile strength of 5.5 ± 1.97 MPa and elongation at break of 3.34 ± 1.6 mm compared to 3.7 ± 2.0 MPa and 1.7 ± 0.7 mm for saphenous veins, respectively, for sample lengths of 1 mm. This outer braided membrane allowed for SMC percolation through the large pores, however SMCs seeding directly from the outside has not been studied.

More recently, the concept of textile-based biomimetic materials for vascular grafts has been extended to fully knitted collagen-based biomaterials[175]. Electrochemically aligned collagen threads were prepared by injecting a collagen solution (3 $mg.mL^{-1}$) between two parallel electrodes mounted on a rotating cylinder, and by imposing a constant electric potential (40 V) to induce the electro-compaction of collagen molecules into filaments (in the pH region corresponding to the isoelectric point). The obtained filaments were combined with PLA to improve mechanical properties and knitted into small-diameter vascular grafts using a circular-knitting machine. Porosity was optimized by adjusting the pull-down tension and the number of filaments for a single thread. Using 3-ply threads (instead of 2-ply yarns) and imposing a higher tension by an increasing weight led to narrower pores. Mechanical properties were assessed and compared to pure collagen and PLA scaffolds. Both the bursting strength and suture retention strength of the hybrid vascular scaffolds were significantly improved compared to the pure collagen ones. Collagen incorporated in the matrix favored cell recruitment compared to pure PLA displaying more than 10 times the number of attached HUVECs, characterized by a more elongated morphology. Evaluation of the scaffold degradation evidenced a gradual loss of weight and tensile strength but displaying sufficient mechanical support at the early stage of cell recruitment, until the regenerated organ assumes this role. This same approach has been recently applied to fully biological knitted scaffolds. Magnan and colleagues developed a new kind of yarn by using cell-assembled extracellular matrix (CAM) sheets produced by normal adult skin fibroblasts[176]. Tubular scaffolds could be directly formed by rolling sheets, or by slicing the CAM sheets into ribbons that were subsequently twisted into threads, dried, spooled and stored as ready-to use biological yarns. A weaving technique was implemented to obtain fully biological grafts, whose dimensional properties could be adapted to various assembling techniques (knitting, knotting, weaving or crocheting), leading to the presence of pores in between the yarns. The resulting material can endure surgical procedure and physiological pressure, with a suture retention strength and burst pressure of respectively 6 N and 6000 mmHg,

compared to 1.4 N and 3000 mmHg for human internal mammary artery. These exciting performances correlate directly with the very dense collagen fibrils network composing the threads. TEM images show their arrangement in parallel bundles and the presence of the typical 67 nm striation of collagen, the hallmark of the physiological fibrillar structures in native tissues[177]. Furthermore, mass spectrometry identified 50 other components of the ECM in the CAM, propelling this material as one of the first biomimetic tubular graft from a compositional perspective. However, the concentration of the ECM components remains unknown. As a proof of concept, a tubular vascular graft was implanted in an ovine model, and even though fully *in vivo* results were not reported yet, suturability, arterial pressure resistance and transmural permeability were confirmed visually and by palpation[176].

The challenges of electrospinning labile biomolecules

As described in section *3.1.4.2*, electrospinning is a versatile method to elaborate different types of porous materials. Using electrospinning to reproduce the microenvironment around smooth muscle cells in the muscular layer of tubular tissues (*i.e.* highly concentrated collagen walls) is complex. The challenge arises from the use of harsh solvents from the dehydration occurring during the process. These parameters have a deleterious impact on the collagen ultrastructure, and need to be considered—and controlled—to elaborate materials that truly are biomimetic.

Most electrospun biomaterials combine biopolymers with synthetic counterparts to achieve a compromise between native biological properties and mechanical strength, respectively[175,178,179]. In particular, gelatin has attracted attention as a low-cost derivative of collagen. Lu *et al.* constructed a three-layered graft[180] composed of an inner PCL/ColI layer, a middle PCL-only layer and a PCL/gelatin outer layer. Spinning solutions were prepared at 10 %wt in 2,2,2-trifluoroethanol at a ratio of (3:1) for PCL/gelatin, and stirred for 24 h. Solutions were gradually spun on a rotating stainless-steel rod covered with aluminum foil, starting from the inner layer. After 4 h of electrospinning, grafts were collected and freeze-dried to remove the solvent. The addition of gelatin in the outer layer increased the hydrophilicity and the fiber diameter with respect to that composed of PCL alone. Although the mechanical properties of the composite material (maximum tensile stress and strain) were greater than those of native tissues (*n.b.* tensile testing was conducted in dry conditions and it is thus difficult to infer the material properties in physiological environment), neither the porosity nor the ability of SMCs to repopulate the scaffolds were evaluated. Despite the interesting properties and the layered structure that captures some features of native tissues reached by this material, questions remain regarding how closely gelatin allows to mimic the native ECM of tubular tissues. Gelatin is a denatured form of collagen as a product of hydrolysis or thermal denaturation, and it is associated with the irreversible loss of the triple-helix secondary structure[188]. The preservation—or not—of the secondary structure determines which

recognition sites are accessible to antibodies. Cell-materials interactions are thus significantly different, and the use of gelatin may induce inflammation and fibrotic tissue formation[181]. Moreover, gelatin lacks the characteristic lyotropic properties of ColI and cannot form fibrillar structures, which are central building blocks responsible for the anisotropy of tubular tissues for the mechanical properties. In 2021 a review article quantified that 53 % of collagen-based electrospun scaffolds reported in the literature were produced exclusively out of ColI[182], the other 47 % being blended with mainly PCL[108,180,183,184]. A common step following electrospinning is the freeze-drying of the material to sublimate the solvent[136] and to obtain a foam or sponge. In the case of type I collagen, this process is known to result in decreased number of α-helices[185] and stiffening of the fibers[41]. The damaging effects inherent to freeze drying can be mitigated by optimizing the freeze-drying conditions (time, pressure, set temperature and temperature gradient)[186].

Choosing the most suitable solvent is also critical in retaining collagen ultrastructure throughout the process. Collagen has a poor solubility in the common organic solvents used in electrospinning, dichloromethane and chloroform, due to its hydrophilicity. Instead, fluoroalcohols are commonly used to dissolve collagen. However, Zeugolis *et al.* demonstrated that using this solvent results in the absence of triple-helix conformation and that the obtained materials exhibited a denaturation temperature lower than fibrillar collagen, comparable to that of gelatin[187]. Resorting to fluoroalcohol-based dissolution created gelatin out of collagen, turning gold into lead. A few studies report the maintenance of collagen ultrastructure after electrospinning, by suspending collagen into acetic acid/DMSO at a ratio of 93/7[188] or 1,1,1,3,3,3 hexafluoro-2-propanol (HFP)[181,189]. Matthews *et al.* collected a concentrated solution of type I collagen (83 $mg.mL^{-1}$) on the mandrel after electrospinning from a short distance (125 mm between needle tip and mandrel)[189]. The short distance facilitated the collection of the spun fibers. Moreover, drying of the collected fibers could result in a concentration range that is comparable to that of native tissues. Cross-linking in presence of glutaraldehyde vapors for 24 h and rinsing in phosphate-buffered saline allowed to restore the fibrillar arrangement of collagen as confirmed by TEM observations, and the effective repopulation by aortic smooth muscular cells after 7 days. However, using cross-linkers results in a different fibrillar arrangement than *in vivo*. To avoid it, pioneering self-standing fibrillar pure collagen scaffolds without the resort to any cross-linker and polymer support were produced by electrospinning, depicted earlier for the recapitulation of the *epithelial inner layer*, page 28[153]. It demonstrates the relevance of electrospinning to elaborate fibrous biomaterials, however the process requires reaching native concentrations, lowering the toxicity by widening the range of solvents, and adjusting the porosity for increased cell migration kinetics.

Controlled porosity through freezing

The elaboration of multi-level hierarchical materials that offer pores, unaltered protein structure and concentration comparable to native tissues, combined with suitable mechanical properties is a gold standard that remains elusive. Freeze-casting or ice templating, is a mild process strategy initially used for the assembly of ceramic green bodies that provides excellent control over the porosity of the resulting materials. The technique has recently been transposed for the elaboration of biopolymer-based cellular architectures[190]. The principle is first to create pores *via* controlled freezing of the aqueous solvent, followed by a second step which consists in sublimating the formed ice crystals to reveal the macroporous structure composed by the solute. The physico-chemical parameters of the solution and the cooling system influence the initial freezing point. During freezing, at equilibrium, bulk water molecules converge to the surface of ice crystals (or nuclei), resulting in a gradual ice crystal growth. During this process, solutes are expelled from the growing ice crystals and concentrate between them[191]. Part of the water remains unfrozen and bound to the solute in a vitreous or glass-like phase[192,193]. Ice can adopt different morphologies that range from fully isotropic up to highly anisotropic lamellar crystals[190]. After sublimation of ice, the pores represent the negative imprint from such structures. As a consequence, the geometry, interconnectivity and orientation of the pores, as well as their size, can be tailored by adjusting the freezing process parameters. The ice growth mechanism is dictated by the thermal properties (thermal conductivity, cooling bath temperature and dipping speed on which depend the temperature gradient and the freezing front velocity), the design of the mold (shape[194], type of material and its thermal properties[195]) and the polymer solution properties (concentration, viscosity, particle size or molecular weight and carrier-particles interactions[196]). A straightforward parameter to tune is the cooling rate. A rapid cooling will translate into small ice crystals and symmetrical pores, whereas a slower cooling will favor the growth of ice crystal along the vertical *c*-axis and yield to larger ice crystals[197,198]. To forecast the porous structure induced by thermal conditions in collagen samples, Cyr *et al*. created a theoretical model that is capable to predict the temperature fields and the corresponding ice growth[199]. The growth of ice-crystals can also be followed *in situ* to understand the impact of ice growth, using a confocal microscope set-up equipped with a cryoscopic stage a solution with a fluorophore[200]. Tailoring the porous structure enables to control the textural characteristics mentioned above. These parameters can be set to encourage cell infiltration and suitable mechanical properties for tissue regeneration[201]. Numerous methods have been developed to control ice formation and growth, including static copper platform[202], rotational freezing[196], controlled dipping[195,203], and translational plane freezing[193,204]. These methods offer to control the macroscopic geometry of the scaffolds (by the design of relevant molds) and, simultaneously allow for a fine adjustment of the macroporosity within the materials via a set of well-defined thermal boundary conditions. Beyond the elaboration of biomaterials, directional freezing techniques have found increasing relevance in the domain of cryopreservation[112]. A few techniques relying on cross-linking are worth mentioning for the ingenuity of the process, although these are not relying on ice-templating. Porogens may be integrated

using for instance gelatin or pluronic F-127 as temporary beads to create pores or complex geometrical structures to support the collagen solution during solidification or cross-linking[205,206]. Foam technology is another efficient way to manufacture porous scaffolds by introducing nitrogen gas bubbles of various diameters in a solution, followed by cross-linking and degassing[207]. Finally, plastic compression methods have been explored to force molecules staggering and densify the material, resulting in increased mechanical properties[208].

The conventional method to sublimate ice crystals following ice-templating is freeze-drying or lyophilization, which results in porous dry materials named foams or sponges[209]. It was briefly introduced in the previous section as a possible additional step for solvent evaporation after electrospinning. However, it can also serve as a standalone fabrication process following freezing of a sample. The drying process can be split into two steps, primary drying (sublimation) and secondary drying (desorption). Yin *et al.* combined a simple ice-templating process and freeze-drying to manufacture highly porous chitosan stents for ureteral replacement[210]. Conductive molds were filled with 3.5% w/v and placed at -80°C to generate a radial bi-directional formation of ice crystals. Molds were subsequently removed and the samples were freeze-dried overnight. Structural analysis by SEM revealed an anisotropic arrangement composed of aligned lamellar pores radially oriented imposed by the mold's conductivity and the homogeneous thermal gradient. The same group of researchers investigated the influence of longitudinal versus radial freezing generated with PTFE or aluminum molds respectively, as well as slow versus fast cooling rate, on pore dimensions[211]. The lamellar spacing, pore area and wall thickness increased with both radial and fast freezing. Poor mechanical performances of the resulting porous materials were compensated by use of chemical cross-linking—a strategy that has equally been applied to collagen-based materials obtained by freeze-drying[212]. Collagenous biomaterials based on ice-templating and freeze-drying are currently used in the clinical, for skin wound healing (extensive burns[213], ulcers[214] and skin defects[215]), osteo-reconstruction[216] or dura matter repair[217].

The challenge after ice-templating lies in removing the ice-crystals by another means than freeze-drying, while inducing the self-assembly of collagen molecules into native-like fibrils. A recent study from Rieu *et al.* introduced for the first time the concept of topotactic fibrillogenesis for the self-assembly of collagen molecules[202]. The strategy is to trigger type I collagen fibrillogenesis after ice-templating, by combining two effects simultaneously: cryoscopic depression of ice in contact with a solute, and the physicochemical conditions (pH rise, ionic force change, etc) able to induce the self-assembly of collagen molecules into fibrils. By exposing the ice-templated scaffolds to ammonia vapors at 0°C, ice was allowed to slowly thaw while the increasing pH forced collagen molecules to form fibrils. Macroporous and anisotropic fibrillar collagen scaffolds were obtained, with regular ridges and pore size. Mechanical performances in the wet state were excellent compared to common cross-linking techniques and close to mammalian soft tissues (33 kPa). Normal human dermal fibroblasts and myoblasts demonstrate high bioactivity (cell adhesion, spreading and myotubes formation) after 11 days

of culture without any additional physical, chemical or biological cues. Similar results were obtained on collagen matrices seeded with fibroblasts for 3D cell culture applications, allowing good proliferation and colonization 7 times further than in equivalent non-porous yet fibrillated matrices at day 28[110]. Moreover, the macroporous matrices presented high dimensional and compositional stability in long-term experiments, reaching up to 60 days of cell culture without noticeable changes. Recently, our team was able to transpose this approach to the fabrication of a variety of collagen-based biomimetic tubular tissues[195]. The ability to control the porosity of both the luminal surface and the muscular layer exclusively using type I collagen yields materials that can accommodate a wide range of cell types and that present elastic properties comparable to hydrated native arteries (from 10 to 58 kPa measured in longitudinal traction). Epithelial and endothelial cells were able to line the luminal side, whereas SMCs and MSCs could effectively migrate from the adventitial side to colonize the tubular sample. The exciting results *in vitro*, together with the mechanical properties and the recapitulation of the fibrillar structures found in native tissues, propel topotactic fibrillogenesis to the most promising strategy to combine with ice-templating for the development of biomimetic tubular tissues.

3D printing

Three-dimensional printing enables the manufacturing of a variety of biomaterials through a gradual building process using hydrogels that allow for geometrical, structural and compositional tunability. The three techniques commonly used are micro-extrusion, inkjet and laser assisted printing[218]. In the context of elaborating soft tissue biomimetic materials, one of the major concerns is to formulate hydrogels that combine printability and high resolution with biocompatibility. Adequate rheological properties of the hydrogels (or of the respective ink prior to hydrogel formation) are central to do so, and include shear thinning, yield stress, viscosity and molding ability. The shear-thinning behavior is characterized by a decrease in the viscosity at high shear ratios, which encompasses a transition from a high-viscosity gel to a low-viscosity fluid during printing. It is followed by a rapid restoration of the gel state to maintain the structural integrity. For each printer-hydrogel combination, the parameters must be carefully adjusted to optimize the structural characteristics of the resulting printed biomaterial. These adjustments include tuning the molecular weight and concentration of polymer, add modifiers, or modifying the bioprinters parameters such as the speed, layering, needle size, among others[219]. Differently from synthetic polymers, ECM-derived bio-inks are studied to optimize the cellular microenvironment and to avoid eliciting an immune response. These factors are deemed essential to promote tissue growth in newly engineered organ[220,221]. It is expected that 3D printing may tackle the issues related with direct implantation of decellularized ECM, by modulating the structure and mechanics of the materials while preserving the native composition. As already mentioned, various sources of ECM are decellularized

and processed into inks, mainly from porcine tissues[221]. One interesting feature of 3D printing is the possibility to perform dual printing and combine several tissue types, as well as to integrate cells

Formulation of dECM bioinks is also investigated for gastrointestinal tract from porcine small intestinal submucosa[222]and urinary tract[223]. To our knowledge, dECM bioinks formulated for vascular tissues are poorly explored[224]—although a few researchers studied the mix of alginate with dECM[225,226]—or rather focused on cardiac tissues[227].

A significant body of work has been devoted to the elaboration of collagen-based bioinks. The major concern with these is their low mechanical properties during the printing process that require additional support to stabilize the printed geometry. To do so, collagen can be printed in molds that are subsequently removed[195], by using printing baths[228,229], or cross-linked following printing[230–232]. An interesting alternative to chemical crosslinking is to increase the ink viscosity by associating it to other biologically derived components (chitosan[233] or gelatin[234]) or by increasing its concentration[235]. However, according to Osidak and co-workers, 90% of the studies carried out on collagen 3D (bio)printing until now use concentrations limited to 10 $mg.mL^{-1}$. These values lay substantially below the concentration of collagen in tissues and fail to provide suitable gel stiffness to ensure geometric fidelity of the printed structure[236]. To tackle this shortcoming, Nociera *et al.* reported the formulation of a collagenous ink at 60 $mg.mL^{-1}$ of lyophilized collagen in PBS, prepared at pH 7[237], that exhibited high viscosity and shear thinning behavior. The low resolution imposed by the high viscosity was skirted by delay times in-between each layer. Two different fibroblastic cell lines demonstrated good adhesion and proliferation on (and later within) the macroporous 3D constructs obtained with a viability of 70%. Another approach was developed by Camman *et al.* to model skeletal muscle ECM, where the acidic solvent of a collagen solution was evaporated until the solution reaches a concentration of 30 $mg.mL^{-1}$[238]. This approach avoids damaging the collagen during the drying step of freeze-drying while still reaching the suitable rheological properties to allow its use as an ink. 3D matrices were printed with a porous architecture (pores of 100 µm). Due to the shearing effect during printing, collagen molecules aligned along the direction of printing when conducted directly in a PBS (5X) bath—to ensure both the geometry stabilization and the collagen fibrillogenesis. Additional channels of 600 µm were created by adding needles in the printed matrix after 30 min fibrillation. After 24 h, an ammonia vapor bath was applied to consolidate the fibrillogenesis and increase mechanical properties. The measured Youngs' moduli ranged from 8 to 25 kPa, which are in the same order of magnitude as that of native ECM. Along with the nutrients' supply provided by the porous network, the matrix stiffness induced the formation of myotubes inside the channels after the seeding with C2C12 muscle cells in Matrigel®. Finally, a recent work may be mentioned for the interesting processing method that it proposes. Named drop-on-demand (DOD), it can effectively generate porosity in a collagen matrix by printing drops directly inside the hydrogel and remove them after stabilization of the structure[239]. Although the two last techniques mentioned above have not been transposed into the elaboration of tubular tissues, they provide important

leads to further develop of biomimetic tubular tissues via 3D printing. An emerging technology named 4D printing could also bring additional properties that enable the formation of tubular structures. The technique relies on the printing of materials with shape-memory properties that respond to external stimuli. The triggers can be either light, temperature or magnetic field, to induce swelling, curvature, self-assembly or disassembly. These features could bring dynamic performances to biomaterials, an interesting perspective to better mimic native tissues[240].

Cryoprinting: coupling 3D-printing and ice-templating

3D printing and ice-templating have been combined to create cryoprinting (also named ice-printing) for the first-time in 2015 by Adamkiewicz and Rubinsky using liquid nitrogen[241], using home-made printing and cooling systems[242]. A custom cryogenic platform was mounted in place of the original printing stage and maintained at a constant temperature and controlled humidity, generally with liquid nitrogen. The substrate was able to move in the Z-axis while the printer head could move in X-Y axes. The molten material was gradually solidified during deposition, forming a well-defined and tunable frozen structure. On the one hand, 3D printing allows to control the macrostructure and adjust the composition of the printout with several inks or cells. On the other hand, the freezing events allow to fix the printed geometry and to form macropores inside the walls, adding a supplementary hierarchical level at the cell length scale. The main challenge with cryoprinting is to find a solvent able to both dissolve the solute and freeze within the temperature range reached by the modified printer, generally between 0 and -80 °C. Ice might also be used as a sacrificial platform or mold,[243,244] instead of a way to create pores. Studies started with synthetic polymers such as PLLA[245], polyhydroxymethylene and polyvinyl carbonate[246], but the field is likely to be extended to biologically-derived material. A few studies have already explored these with coaxial cryoprinting of a core-shell structure using alginate and PCL, respectively[247], or PCL only dissolved in glacial acetic acid[248]. Several set-ups have been reported as suitable for cryoprinting, including printing in a cooling fluid[241], in a cryogenic chamber with liquid nitrogen-filled walls surrounding the printing stage[243], or atop different cooled platforms (provided with a solid CO_2 in isopropanol reservoir[246,249], an inner circuit filled with alcohol at -20°C[247], or simply a cooled copper plate[244]). Removal of ice while preserving the porosity has been done by phase separation based on DMSO polymeric solution/water bath interactions[246] or by standard freeze-drying[247,248]. The cryoprinted materials exhibit a well-defined structure providing different levels of organization, proven to enhance cellular proliferation compared to traditional printed technique[248], especially if using additional biocompatible fillers such as crosslinked gelatin nanofibers[246]. Considering the narrow research field of cryoprinting, type I collagen has taken very little attention. Concentration of 4.5% w/v in acetic acid was used by Kim *et al.* on a home-made set-up named “3D plotted system” that was basically a 3D printer equipped with a cryogenic stage, to create squared porous samples[242]. After freeze-drying,

authors investigated the structural features and mechanical properties, and the influence of process parameters on the obtained materials. Extensive research using cryoprinted collagen combined to softer fibrillogenesis methods, as detailed in the previous section, seems promising in the field of tissue engineering.

3.2.2 Dense materials promoting cell adhesion and material remodeling

Cell-mediated ECM shaped into dense tubular structure

Some cell types are able to produce ECM under adequate culture conditions. This property has been exploited to produce cohesive cell sheets both *in vivo*[250] and *in vitro*[176], to engineer epithelial layers as discussed above and larger 3D structures. These sheets are comprised of living cells in a complex mix of biological material, which can be detached from the culture plate for further modeling. Methods to shape these sheets into thick tubes include wrapping[251], layer-by-layer assembly[30], ring-stacking[252] and textile-inspired techniques[176] (read section *3.2.1.1* for more details). Most cell sheets are generated *in vitro* for practical reasons, but it is also possible to generate matrices by relying on the capacity of living tissues to generate biological substrates. Yamanami *et al.* implanted molds sub-cutaneously in dog dorsal skin for 4 weeks, and obtained tubular connective tissues after harvesting[250]. However, this technique is ethically questionable in an industrial context in view of the current regulatory framework. Aside from commercialized commodity, cells can also be sourced directly from patient biopsies and expanded *ex vivo*. This was demonstrated for the first time by L'Heureux *et al*. who fabricated a biological and clinically effective material from autologous cells for small-diameter arterial replacement[253]. They used fibroblast-derived ECM sheets, which were simply wrapped around a temporary Teflon®-coated stainless-steel tube. After a maturation step of 10-weeks, layers were cohesive and formed a homogeneous tissue. The final material was fabricated with two thick layers based on this method. A living cell sheet was used as the external layer to provide stiffness while the middle layer consisted in a decellularized sheet to limit cell migration towards the lumen. Finally, ECs were seeded on the luminal side to form the endothelium. The final material was proven non-thrombogenic and featured mechanical properties in the range of native tissues *in vitro*. *In vivo* experiments in rat model confirmed the ability to regenerate an endothelium displaying a barrier function, promote SMC infiltration, and reform the characteristic *vasa vasorum* and the basal membrane. The materials thus seem to be able to replace arteries from autologous cells, but result in a particularly lengthy process. Another study succeeded in shortening the fabrication time by simplifying the model to directly produce a contiguous bi-cellularized sheet containing both SMCs and fibroblasts[254], and which can be further rolled. Biological properties were not assessed but the mechanical properties were higher than the standard association of two different cell line sheets, including burst pressure and linear modulus, enabling the material to sustain physiological vascular pressures.

A different study has focused on optimizing the balance between two cell lines, using a hybrid technique that combines sheet-stacking and reseeding[255] for urethra replacement application[256]. This method enables to solve the common unbalanced properties of cell-generated matrix, which provide adequate mechanical properties but do not preserve the epithelial layer barrier function. In the case of urethra, it is crucial to avoid inflammation and fibrosis originating from urine extravasation. Two cell sources of fibroblasts were investigated to produce the stroma, vesical fibroblasts (VF) to support epithelium formation, and dermal fibroblasts (DF) to improve mechanical properties. These were used either as a single source, or mixed in various ratios (VF only, 90/10, 80/20, 70/30 corresponding to VF/DF, and DF only), and their impact on urothelium formation from seeded urothelial cells (UCs) was assessed. For the study, both fibroblasts and epithelial cells were extracted from human bladder biopsies, which provide similar UCs while avoiding the significant co-morbidities associated to urethral biopsies. Fibroblasts were seeded with ascorbate on well plates and cultured for 28 days with a reseeding at day 14 to obtain neosynthesized ECM sheets. After sheet stacking, the stromal sheets were subsequently seeded with urothelial cells. After 7 days, the substitutes were detached from the bottom of the plate to reach the air-liquid interface and induce mature urothelium differentiation. The final structures demonstrated that high concentrations of VF (80 to 90 %) significantly improve impermeability towards urea, mechanical properties, and the near-restoration of the endothelium and basal lamina. Interestingly, villi were observed for all samples comprised with VF. Tubularization of the flat materials was not tested as the common grafts implanted for urethroplasty are flat.

Instead of wrapping a single layer around a tube, multiple cell layers can be assembled by a layer-by-layer (LbL) process[30]. 3D dense tissues with high cell density are built by gradually overlaying multiple SMC layers from previously expanded SMCs brought to confluence. Between each deposition, a thin coating of ColI was applied to favor attachment between adjacent layers. After one week, a five layers-tube was fabricated, exhibiting elongated SMCs aligned in the direction of the microchannels. After two weeks, the thickness of a human coronary artery could be reached, corresponding to the equivalent of 10 assembled layers. Optimization of the technique was proposed by Xu *et al.*, who directly produced tubular material from cell expansion[257].

Patel et al. developed a ring stacking method to generate biomimetic arterial *tunica adventitia*[252]. Tissue rings were self-aggregated around center posts and stacked into a tubular structure. The base plate was fabricated using PDMS posts, coated with fibrin gel only (20 $mg.mL^{-1}$) or a combination in various ratios of fibrin and collagen (0.7 to 2.2 $mg.mL^{-1}$) . Expanded human dermal fibroblasts (hDF) were then seeded onto the posts and cultured for 7 days. Stimulation of the collagen production was not only explored through the supporting matrix, but also by continuous additions of factors. These cytokine stimulating agents included TGF-β, ascorbic acid (AA) and combinations of both at various timepoints. At day 7, the self-assembled fibroblasts mediated rings were removed from the plates and 6 of them were placed

around a rod. Cohesion of the overall tubular construct was ensured by a simple sealing of the rings with fibrin glue composed of fibrinogen and thrombin, enabling the use of the grafts after 8 days only. The continuous stimuli by cytokines promoted collagen production associated with a significant increase in the mechanical properties. In particular, the combination of TGF- β and AA resulted in the thickest ring and highest cell density, associated with the highest elasticity, ultimate tensile strength, and failure strength. Compared to rings supported by fibrin alone, fibrin-0.7 $mg.mL^{-1}$ collagen mediated rings were significantly denser, with twice as much collagen content. The cell density was continuous along the tube that demonstrated good cohesion in between the rings. The same method was applied to SMCs with the intention of forming a tubular muscular layer[258], which could be integrated as the *tunica media* for arterial replacement, or may be used alone for other tissue types. Versatility of the layering method allows to use various type or cells, orient cells differently for each layer or create various topographies. Xu *et al.* have illustrated the advantages of the technique by producing an arterial outer layer featuring helicoidally-oriented SMC, reproducing the native arrangement of muscular cells in the native tissue[257].

The cell-sheet engineering research community has mostly focused on vascular applications, hence the results presented here are mostly driven by this final application. However, similar techniques are used for other tubular tissues and a few examples are reported for each in **Table 4**.

Densification of collagen

Most tubular scaffolds fail to reach the concentration of ColI in native tissues. To address this issue, Justin *et al.* developed a densification method that generates a new type of highly concentrated collagenous tubular materials[259]. The resulting tubes are seamless, provided with relevant mechanical properties and display homogeneous fibril density along the tube. The authors used a funnel-shaped chamber composed of a central rod and an outer mold, laying on hydrophilic porous nylon membranes on top of paper-towel. Gradual withdrawal of the water from the bottom combined to water repelling from the pores thanks to collagen contraction anchorage in the membrane, enabled to reach a collagen concentration ranging from 120 to 190 $mg.mL^{-1}$, depending on the initial concentration and volume. Second harmonic generation (SHG) images revealed a network of collagen fibrils and fibers aligned along the axis of the walls. Upon crosslinking with genipin at low concentration (1 mM) the resulting materials displayed a 2 to 3-fold increase in tensile strength. The method has proven efficient in directly integrating cells and maintaining their viability and, more interestingly, in tailoring the cells' spatial distribution both for single and multiple-cell type experiments. This versatility may allow to recreate the distinct cellular spatial configuration of the aorta with endothelial cells in the luminal part and smooth muscle cells on the outer part for instance. Additionally, the central rod surface can be tailored to resemble native luminal patterns such as the wavy motifs of arteries of the crypt-villi texture of gastrointestinal tracts.

Another study developed a micro-fluidic device to extrude collagen sheets and increase collagen compaction[260]. The principle lies in the co-extrusion of a collagen solution in between two layers of a flow focusing buffer (FFB) inducing pre-fibrillogenesis. Collagen fibrils are aligned in the direction of the extrusion by a continuous strain using a rotating mandrel, followed by a buffer bath to complete fibrillogenesis. Collagen solution was prepared by dissolving lyophilized ColI in deionized water at a concentration of 5 $mg.mL^{-1}$, and the FFB was composed of PEG and salts. An adjustment of the pH to 8 promoted the self-assembly of collagen molecules by increasing the pH close to their iso-electric point (*ca.* 7.4) and enabling increased hydrophobic interactions between the molecules. PEG, a crowding agent, was used to favor the expulsion of water by providing a hypertonic environment. Additionally, collagen sheet was strained by a rotating mandrel over which it passes to induce fibril alignment, and fibrillogenesis was then completed by a buffer solution bath for 48 h. Finally, the sheet was washed and dried to increase compaction. Through shear, strain, macromolecular crowding and evaporation, this device enables to produce highly concentrated collagen layers with a native-like ultrastructure. Ability of the material to support cell proliferation was evaluated using ECs and SMCs, and influence of the degree of fibrillar alignment controlled by the extrusion speed was explored. Coordinated vasoconstrictive and vasorelaxation responses were only observed for co-aligned SMC-sheets, providing higher contractile and residual stresses. This approach proposes unprecedent features of native collagen found in the ECM, *i.e.* high compaction and native ultrastructure, while being an easy and fast process.

Loy *et al.* developed a novel technique based on a rotational bioreactor that expels water and densifies collagen to produce tubular scaffolds[261]. The method consists in filling a tubular mold with 2 $mg.mL^{-1}$ ColI solution, dissolved in acetic acid, Dulbecco's modified Eagle's medium (DMEM), NaOH and Hepes to induce fibrillogenesis. The outer mold was further removed to place the matrix on a homemade rotating bioreactor in an incubator at 37°C for 1 h. Rotation enabled to align fibrils in the longitudinal direction while expelling water. A four-fold increase in concentration was measured, resulting in significant improvement in the mechanical properties. The possibility to incorporate cells in the process was evaluated using fibroblasts, and demonstrated steady cell viability before and after rotation. This versatile technique is particularly adapted to prepare tubular matrices. Moreover, it allows for the assembly of biomimetic components of the ECM into hierarchical or multi-layered structures capable of hosting various cell types.

Collagen as a bioink to generate cellularized tubular grafts

In parallel with the control over the geometry of the printed objects, the possibility to use biomimetic components as printing inks and the capacity to co-print different compositions, 3D printing has the

ability to directly integrate cells during the fabrication process, a now widespread technique called bioprinting[29]. Bioprinting enables to incorporate cells in a hydrogel with a precise control over their spatial distribution in a material. For tracheal tissue engineering, it opens up an exciting opportunity to create alternating rings of tissue-specific bioinks that promote either cartilage (C) or vascularized fibrous (VF) tissue regeneration[262]. Photocrosslinkable inks were developed by incorporating cells into dedicated ECM-derived inks both sourced from pigs. For the C-ink, chondrocytes were loaded in a hydrogel composed of methacryloyl-modified gelatin, chondroitin sulfate, and cartilage acellular matrix. For VF ink, fibroblasts were loaded in a vascularized fibrous tissue bioink composed of methacrylate-modified hyaluronic acid, 8-arm-polyethylene glycol-succinic acid ester (8-PEG-NHS), and methacryloyl-modified dermal acellular matrix. Upon photo-initiation, the temperature-sensitive C ink became stiffer while the highly viscous VF ink remained soft, forming a stiff-to-soft ring staggered structure. Seamless interfacial fusion of adjacent rings was ensured by amidation of the 8-PEG-NHS. The resulting tracheal analogs demonstrated good mechanical properties and suitable cellularization. The alternating structure, with cartilaginous and vascularized fibrous tissue rings, offers a combination of mechanical resistance (compressive resistance, tensile and bending ability) and sufficient nutrients supply. It enabled the restoration of its functionality following tracheal implantation in a rabbit model. Using a comparable approach, Nam *et al.* proposed a modified bioprinting set up for esophageal reconstruction, with an inner mucosal layer and a muscular outer layer[263]. The main difference relies in the possibility to create pores in the material to favor cell migration. To achieve this, the authors developed a dragging technique able to print altered lines with adjustable width and pore size in a single step. The resulting esophagus mime facilitates cell proliferation thanks to its multilayered porous structure, as confirmed by *in vitro* experiments using SMC.

The central challenge in bioprinting is to ensure the survival of cells, which face confinement in the syringe as well as exposure to isostatic pressure and shear forces during printing. Through modulation of the type, source and density of cells, diverse heterogeneous constructs can be fashioned to mimic various native tissues, for instance arterial tissue by combining human aortic SMCs and HUVECs[264].

Diamantides *et al.* studied cell viability and activity using chondrocytes in a 8 $mg.mL^{-1}$ type I collagen bioink directly after bioprinting, and up to 14 days[265]. Assays demonstrated cell viability over 90% from day 0 until the end of the culture period. By day 11, noticeable shape retraction of the matrices was observed, highlighting the biological activity of cells but also the insufficient collagen concentration to ensure dimensional stability. Authors also demonstrated that cell density impacts rheological properties of the bioink. The shear-thinning behavior was steady across all cell concentrations, however increased cell density led to higher storage modulus prior to printing, but reduced moduli in the gel state (following printing and gelation at 37°C). The introduction of cells into the ink also led to improved resolution compared to acellular ink, resulting in reduced dot footprint and narrower line widths. However, as rheological properties depend on the cell type due to variations in cell size and their interactions with

the chosen hydrogel, these findings should be taken cautiously. Multicellular spheroids may also be used instead of single cell lines to replicate the native cellular population[266].

The examples just above point out to the relevance of collagen as a bioink in terms of cell viability. This same argument has equally drawn attention in the context of tubular tissue applications [267]. Nevertheless, collagen-based bioinks often require pre- or post-processing: either a crosslinking step, lyophilization prior to dissolution[268], or a modification of the composition by the addition of components that are not part of native tissues such as alginate, methacrylated gelatin, PEG or PCL[269]. These changes participate to increasing the mechanical stability of the printed constructs and, in most cases, to lowering the cost of fabrication and explain the scarcity of research projects focusing solely on pure collagen[270].

Rué *et al.* developed a core-shell structure composed of an inner alginate-ColI-HUVECs layer and an outer ColI-human aortic SMCs layer using a triple coaxial nozzle to mimic arteries[264]. For the luminal layer, HUVECs were simply suspended at a density of 15.10^6 cells.mL^{-1} in a 5 mg.mL^{-1} collagen solution. For the outer layer, SMC were encapsulated at a density of $10x10^6$ cells.mL^{-1} into a solution of alginate (2%wt) and collagen (3 mg.mL^{-1}). The two layers were co-printed with a central pluronic F-127 ink to create the lumen, directly in a Ca^{2+} solution at 37°C. Maintenance and stiffening of the scaffolds were secured by calcium ions that induced alginate crosslinking, and by the increased temperature that induced collagen gelation. Pluronic support was dissolved in water for co-culture of the scaffold over 14 days. The shear stress exerted during the process had no detrimental impact on cell viability and, by the fifth day, HUVECs had formed a monolayer whereas SMCs displayed a rounded morphology that deviated from the native contractile phenotype. The differences in behavior may be attributed to the lower collagen concentration in the outer layer. However, SMCs exhibited a diagonal-perpendicular alignment akin to the perpendicular alignment observed in native arteries. Another interesting result was that cells did not intermingle and remained in their respective layers. The comparable results obtained with dECM and ColI suggest that the single component ColI bioink could be advantageous[226]. A similar co-extrusion method increased mechanical strength by using eight-arm PEG acrylate and gelatin methacryloyl rather than ColI[271]. The scaffold effectively promoted bladder urothelial cells proliferation and urothelium reformation in the inner layer, meanwhile on the opposite side cells expressed α-smooth muscle actin, the predominant isoform in vascular smooth-muscle cells which plays a key role in fibrogenesis.

In a study by Kim *et al.*, the authors prepared a gastrointestinal model by loading cells into a pure collagen scaffold through bioprinting and crosslinked wih tannic acid (TA)[272]. To prepare the tubular construct, a 4%wt collagen bioink was loaded with HUVECs in the shell layer and with Caco-2 (epithelial) cells in the core layer, both at a cell density of $5x10^6$ cells.mL^{-1}. The high amount of added TA enabled to precisely build a stable intestine-like architecture and to obtain micro-vascular structures with the shell ink, while lower quantity of TA in the core ink ensured a good coverage by Caco-2 cells.

The resulting co-cultured scaffold presented outstanding structural similarities with GI tracts, and the presence of the capillary network increased cell proliferation, enzyme expression, and barrier function.

Post-fabrication perforation to enhance dense materials biointegration

Alternatively, enhancing cell migration in a scaffold may be done by generating porosity with a post-fabrication perforation. A method was introduced by Marzaro *et al.* for esophageal replacement, using a patented microscopic robotic perforator. After decellularization and removal of the submucosa and mucosa of a porcine esophagus, the remaining muscular layer was perforated with a 150 µm needle. An algorithm controlled the regularity of the pattern, to obtain about 1200 pores/cm² and a pore size ranging from 80 to 100 µm with a similar interspace. The scaffold dimensions, thickness and ECM architecture were preserved, and no burns or damages of the connective tissue were observed. After culturing autologous bone marrow-derived mesenchymal stromal cells for 10 days, SEM images showed that cells adhered and diffused in the inner and outer layers of the scaffold. *In vivo* studies using pigs evidenced that after 3 months, the muscular layer was regenerated for pre-seeded scaffolds, while it was not the case for non-seeded scaffolds. However, half of the pigs suffered from non-practicable stricture in both groups, and substenosis occurred at a higher rate with pre-seeded scaffold[106].

Cell ingrowth can also be enhanced through laser micro-perforation, as demonstrated by Xu *et al* [273]. Trachea matrices were perforated with a laser, optimized to find the right balance between pore dimensions and structure conservation. Such parameters included output power, pulse width, and number of cycles. The resulting lattice-arranged conical pores were spaced 1 mm apart, with a maximum pore size of 800 µm, and no significant damage on the ECM was evidenced by H&E staining. Pores enabled a rapid and efficient decellularization, and the interconnected network facilitatds infiltration and proliferation of chondrocytes in the micropores and bilateral surfaces. *In vivo*, after 3 months implantation on porcine models, this rapid cell infiltration led to a regenerated cartilage twice as thick as for a native trachea, and with higher mechanical strength.

3.2.3 Advantages & disadvantages of each technique

In this section, we described various fabrication methods to reproduce the muscular layer of tubular tissues with a focus on pure type I collagen materials. We identified two main approaches, either *porous* materials facilitating cell migration or *dense* materials promoting cell adhesion and matrix remodeling, illustrated in **Figure 4** and detailed in **Table 4**.

Table 4. Comparison of various methods for biomimetic tubular tissue muscular layer elaboration. Advantages and disadvantages as well as referenced research work are given to provide guidance in its fabrication.

Method	Advantages	Disadvantages	Ref. for the circulatory system	Ref. for trachea	Ref. for GI tracts	Ref. for esophagus	Ref. for urinary tracts	Non-tissue specific
Porous materials								
Decellularization	Preservation of the native tissue architecture and composition	Materials are not always compliant, fail to reach mechanical properties comparable to native tissues.	165,166,171,274,275	163	276,277	278,279	Bladder: 280	N/A
Textile-inspired	Composition similar to the ECM, tunable geometry.	Long process to obtain the threads or ribbons. Compliance not suitable for physiological function.	175,176,281	N/A	N/A	N/A	N/A	N/A
Electrospinning	Easily scalable, possibility to create an entanglement of several components, tunability of the porous network (size, orientation, interconnectivity).	Difficulties to electrospun pure collagen and maintain its native structure throughout the process. The solvents, drying, freeze-drying, and/or cross-linking can induce collagen denaturation or limit the molecular self-assembly.	108,179,180,184	N/A	282	N/A	146	153,178,189

Freezing techniques	(a) Freeze-drying Easy and tailorable process to generate porous structures, with pore size suitable for cell colonization. (b) Topotactic fibrillogenesis Porous network combined to dense collagen walls with a native-like fibrillar ultrastructure.	(a) Freeze-drying Weak mechanical properties associated with walls too thin to support SMCs colonization and contraction. Additionally, collagen is not in a fibrillar form, requiring chemical cross-linking. (b) Topotactic fibrillogenesis The competition between the kinetics of ice thawing and collagen self-assembly may lead to pore size and volume reduction. Recent method, with no *in vivo* results yet.	[283]	(a) [284,285]	(a) [286]	(a) [287]	(a) [210]	(a) [190,209,211] (b) [202]
3D-printing	Tunable geometry, possibility to use several inks in the same material to create layers or rings.	The bioink should enable high resolution printing, and adequate mechanical properties that are often yield by using cross-linkers. The high viscosity of dense collagen also hamper printing in the physiological concentration range.	[225,226]	[262]	[222]	[263]	[223]	[221,237–239,275]

Cryoprinting	High-resolution fabrication technique, enabling to tune the porosity, the number of layers and the complex composition.	Requires to build a homemade set-up controlling both temperature and humidity to ensure printability. Removal of ice without compromising the printed structure is challenging	N/A	N/A	N/A	N/A	N/A	241–244,246–249
Dense materials								
Cell-mediated ECM fabrication	Self-assembly process that generates endogenous biological materials with a composition and an architecture almost equal to native tissues, as opposed to any other process.	Cell sourcing issues (biocompatibility and availability) associated with long production times.	47, 262,263,266,295	289	290	291	159,256	N/A
Densification	Easy method to provide increased mechanical properties and a physiological concentration range, while preserving the ability of molecules to self-assemble.	Require to develop homemade setups.	259,261	N/A	N/A	N/A	N/A	259–261

Bio-printing	Biocompatible, suitable for cell integration and easily printable.	Long optimization of the bioink rheological properties, due to printability issues and insufficient mechanical properties.	264,269,292	293,294	272	266,295	271	Reviews on collagen-based bioinks: 236,265,267,270

Conclusions

Tubular tissues share common structural and compositional features. Their structure can be described with a simplified dual-layer model, comprising the epithelial inner layer and the muscular outer layer. While the first provides impermeability towards the inner wall, as well as absorption and exchange properties, the latter is responsible for structural stability, hosting the smooth muscle cells, and for the overall mechanical properties.

Type I collagen is the main building block of native tubular tissues. The arrangement of this protein is governed by self-assembly processes of the molecules, mediated by physico-chemical parameters that include concentration, pH and ionic strength. The ability to reproduce its conformation and concentration as found in vivo, is the leading pathway to mimic and eventually to replace native tissues. We have thus devoted a large part of this review article to methods based on type I collagen or ECM-derived material. Besides, the shape of tubular tissues poses substantive challenges to many materials processing techniques, which required a myriad of adaptation strategies. Formulating a material that combines both the native structure and composition defines the biomimetic approach, a term that we clarified in the introduction. Strategies to yield both a biomimetic composition and a biomimetic structure can be placed in a two-axis graph, drawn to guide the fabrication as well as a framework to compare different approaches reported in the literature.

To reform an epithelium, we identified three main strategies relying on structural or biological modifications of the luminal surface. ECM-derived surfaces, bioactive surfaces, and textured surfaces propose methods with similar results in terms of cellular adhesion and proliferation, which promote the material biointegration. ECM-derived surfaces are based on native ECM from autologous grafts, decellularized ECM, or cell-mediated ECM production. In addition, pre-seeding of grafts or in situ transplantation of cells enables an efficient re-epithelialization. In order to enhance epithelialization in situ, strategies that take inspiration from the basal membrane—by the addition of luminal protein coatings or active biomolecules—have proven efficient. The increased number of binding sites improves cell adhesion and proliferation, resulting in enhanced epithelialization with respect to the nude material. Finally, textured materials featuring fibers or specific topographies can direct cells spreading and improve their adhesion in vivo.

Multiple strategies have been developed to mimic the muscular outer layer as it is the constitutive layer of tubular organs. We classified these methods into two approaches: one relies on a porous network that facilitates cell and nutrients diffusion for the reconstitution of the entire tissue complexity, while the other hinges on dense matrices with increased compositional complexity. These two visions stand opposite, with the former that seems to show greater success, ease of

process, and fewer biocompatibility issues. Porous materials can be achieved by decellularizing native tissues, braiding cell-derived ECM sheets, or building 3D porous materials from type I collagen via electrospinning, ice-templating, 3D-printing, or cryoprinting. Dense muscular layers, on the contrary, rely on the cells ability to remodel the surrounding matrix. The latter can be either produced directly by cells (i.e. fibroblasts), or resulting from densification or bioprinting methods. These processing methods are particularly interesting since they allow introduction of relevant cell lines for each layer, for instance epithelial cells and smooth muscle cells.

The question that motivated this review is twofold. i) What are the key characteristics that remain unaddressed in the attempts to mimic and to replace native tubular tissues? ii) Which processing techniques are expected to tackle the current shortcomings and produce next-generation of biomaterials for clinical applications? In terms of technical means, building biomaterials, particularly those that encompass biological components—living or extracted from mammals—poses significant challenges in terms of their translation to clinical use, owing to the regulatory framework and the lengthy steps prior to clinical studies. Despite significant progresses in emulating living tissues in the lab, the intricate native cellular microenvironment, the structural and mechanical features, and the need to consider the organisms' homeostatic mechanisms raises many questions about the significance of in vitro models and their relevance in vivo. Approaches based solely on the use of biopolymers have demonstrated superior outcomes, particularly porous materials. In that sense, the techniques of ice-templating, electrospinning, and cryoprinting emerge as versatile tools with good reproducibility. Regarding the epithelium restoration, textured surfaces or protein coatings are straightforward routes to foster ECs adhesion and proliferation. Future developments of tubular tissues should combine a porous network with an engineered luminal surface, in a matrix composed of native-like type I collagen or ECM-derived material. Furthermore, it is worth noting that some tubular tissues, such as respiratory and urinary tract and notably urethra and ureter, have received relatively limited attention from both the biomaterials' community for their reproduction and the basic biology community for their in-depth description. However, there is a growing clinical demand for effective treatment of these tissues. We believe that this will push the scientific community to delve further into these tissues, propelling these as the next topics of biomaterials research in the upcoming years.

Conflicts of interest

There are no conflicts to declare.

References

1 A. Góra, D. Pliszka, S. Mukherjee and S. Ramakrishna, *J Nanosci Nanotechnol*, 2016, **16**, 19–39.

2 P. G. Camici, C. Tschöpe, M. F. Di Carli, O. Rimoldi and S. Van Linthout, *Cardiovasc Res*, 2020, **116**, 806–816.

3 B. W. Warner, *Cell Mol Gastroenterol Hepatol*, 2016, **2**, 429–438.

4 Z. Ungvari, S. Tarantini, A. J. Donato, V. Galvan, A. Csiszar, C. Impairment, N. Program, O. City, O. City, A. Medical, C. L. City, S. L. City, A. Studies and S. Antonio, *Mechanisms of Vascular Aging*, 2018, vol. 123.

5 S. Bruhin-feichter, W. Meier-ruge, G. Martucciello and E. Bruder, .

6 J. P. Richalet, *Rev Mal Respir*, 2021, **38**, 395–403.

7 B. Amadi, K. Zyambo, K. Chandwe, E. Besa, C. Mulenga, S. Mwakamui, S. Siyumbwa, S. Croft, R. Banda, M. Chipunza, K. Chifunda, L. Kazhila, K. VanBuskirk and P. Kelly, *Nat Microbiol*, 2021, **6**, 445–454.

8 M. D. Gerhard-Herman, H. L. Gornik, C. Barrett, N. R. Barshes, M. A. Corriere, D. E. Drachman, L. A. Fleisher, F. G. R. Fowkes, N. M. Hamburg, S. Kinlay, R. Lookstein, S. Misra, L. Mureebe, J. W. Olin, R. A. G. Patel, J. G. Regensteiner, A. Schanzer, M. H. Shishehbor, K. J. Stewart, D. Treat-Jacobson and M. E. Walsh, *Circulation*, 2017, **135**, 686–725.

9 H. Wessells, A. Morey, L. Souter, L. Rahimi and A. Vanni, *Journal of Urology*, 2023, **210**, 64–71.

10 H. Kuwano, Y. Nishimura, T. Oyama, H. Kato, Y. Kitagawa, M. Kusano, H. Shimada, H. Takiuchi, Y. Toh, Y. Doki, Y. Naomoto, H. Matsubara, T. Miyazaki, M. Muto and A. Yanagisawa, *Esophagus*, 2015, **12**, 1–30.

11 F. Matsumoto and K. Ikeda, *Cancers (Basel)*, 2021, **13**, 1–13.

12 M. Carrabba and P. Madeddu, 2018, **6**, 1–12.

13 J. Sánchez-Ibañez, C. Humphreys, M. Lomero, M. Escoto, M. J. Weiss, M. Wilson and M. López-Fraga, *Transplant Direct*, 2023, **9**, e1466.

14 A. H. Blakemore, A. B. And, N. Voorhees and N. Y. York, .

15 N. Pien, S. Palladino, F. Copes, G. Candiani, P. Dubruel, S. Van Vlierberghe and D. Mantovani, *Cells Tissues Organs*, 2022, 128–154.

16 M. C. Lai and A. Latif Ibrahim, *Physiology and reproduction*, 1982, **63**, 1425–1431.

17 H. M. Shields, R. A. Sawhney, F. Zwas, J. A. Boch, S. Kim, D. Goran and D. A. Antonioli, *Microsc Res Tech*, 1995, **31**, 248–256.

18 D. Hopwood, G. Milne and K. R. Logan, *J Pathol*, 1979, **129**, 161–167.

19 J. J. Barboriak, D. L. Van Horn and K. Pintar, *Journal of Thoracic and Cardiovascular Surgery*, 1976, **71**, 673–679.

20 Orlandini G. E., S. Z. Orlandini, A. F. Holstein, R. Evangelisti and R. Ponchietti, *Andrologia*, 1987, **19**, 315–321.

21 M. Woldemeskel, W. Drommer and M. Wendt, *Anat Histol Embryol*, 1998, **27**, 51–55.

22 P. G. Toner, K. E. Carr, A. Ferguson and C. Mackay, *Gut*, 1970, **11**, 471–481.

23 J. S. Trier and C. E. Rubin, *Gastroenterology*, 1965, **49**, 574–603.

24 K. N. Bitar, S. Raghavan and E. Zakhem, *Gastroenterology*, 2014, **146**, 1614–1624.

25 F. Taraballi, M. Sushnitha, C. Tsao, G. Bauza, C. Liverani, A. Shi and E. Tasciotti, *Adv Healthc Mater*, 2018, **17**, 1–13.

26 S. S. M. Rensen, P. A. F. M. Doevendans and G. J. J. M. Van Eys, *Netherlands Heart Journal*, 2007, **15**, 100–108.

27 J. H. Kristensen and M. A. Karsdal, *Chapter 30 - Elastin*, Elsevier Inc., 2016.

28 N. K. Karamanos, A. D. Theocharis, Z. Piperigkou, D. Manou, A. Passi, S. S. Skandalis, D. H. Vynios, V. Orian-Rousseau, S. Ricard-Blum, C. E. H. Schmelzer, L. Duca, M. Durbeej, N. A. Afratis, L. Troeberg, M. Franchi, V. Masola and M. Onisto, *FEBS Journal*, 2021, **288**, 6850–6912.

29 C. Parisi, K. Qin and F. M. Fernandes, *Philosophical Transactions of the Royal Society A: Mathematical, Physical and Engineering Sciences*, DOI:10.1098/rsta.2020.0344.

30 Y. L. Mary B. Chan-Park, Jin Ye Shen, Ye Cao, Yun Xiong and H. P. G. Shahrzad Rayatpisheh, Gavin Chun-Wei Kang, DOI:10.1002/jbm.a.32318.

31 L. Chen, C. Yan and Z. Zheng, *Materials Today*, 2018, **21**, 38–59.

32 L. S. Nair and C. T. Laurencin, *Progress in Polymer Science (Oxford)*, 2007, **32**, 762–798.

33 M. Vert, *Progress in Polymer Science (Oxford)*, 2007, **32**, 755–761.

34 L. Yang, H. Wu, L. Lu, Q. He, B. Xi, H. Yu, R. Luo, Y. Wang and X. Zhang, *Biomaterials*, DOI:10.1016/j.biomaterials.2021.121055.

35 E. Jones, T. Jensen, I. Sharma, H. Wanczyk, A. Mitchell, C. Foster, W. Sayej and C. Finck, DOI:10.1016/B978-0-08-102561-1.00023-3.

36 L. Elomaa, M. Lindner, R. Leben, R. Niesner and M. Weinhart, *Biofabrication*, , DOI:10.1088/1758-5090/ac9433.

37 J. Li, K. Zhang, H. Chen, T. Liu, P. Yang, Y. Zhao and N. Huang, *Materials Science and Engineering C*, 2014, **38**, 235–243.

38 Z. Wang, M. Li, B. Wang, Y. Xu, J. Li, S. Zhang, Q. Qin and J. Wang, .

39 X. Zhang, X. Chen, H. Hong, R. Hu, J. Liu and C. Liu, *Bioact Mater*, 2022, **10**, 15–31.

40 M. Asgari, N. Latifi, F. Giovanniello, H. D. Espinosa and M. Amabili, *Adv Nanobiomed Res*, 2022, **2**, 2100159.

41 Peter Fratzl, *Collagen structure and mechanics*, Springer, 2008.

42 J. A. Last and K. M. Reiser, *Environ Health Perspect*, 1984, **VOL. 55**, 169–177.
43 L. Salvatore, N. Gallo, M. L. Natali, A. Terzi, A. Sannino, M. Madaghiele and M. G. Raucci, , DOI:10.3389/fbioe.2021.644595.
44 M.-M. Giraud-Guille, E. Belamie, G. Mosser, C. Helary, F. Gobeaux and S. Vigier, *Comptes Rendus Chimie*, 2008, **11**, 245–252.
45 G. Mosser, A. Anglo, C. Helary, Y. Bouligand and M. M. Giraud-Guille, *Matrix Biology*, 2006, **25**, 3–13.
46 M. M. Giraud-Guille, *Int Rev Cytol*, 1996, **166**, 59–101.
47 J. Charvolin and J. F. Sadoc, *Interface Focus*, 2012, **2**, 567–574.
48 F. Portier, C. Teulon, A. Nowacka-Perrin, F. Guenneau, M.-C. Schanne-Klein and G. Mosser, 2017, 12916–12925.
49 S. Gorgieva and V. Kokol, *Biomaterials Applications for Nanomedicine*, , DOI:10.5772/24118.
50 D. A. Knight and S. T. Holgate, *Respirology*, 2003, **8**, 432–446.
51 S. Mishani, H. Belhoul-Fakir, C. Lagat, S. Jansen, B. Evans and M. Lawrence-Brown, *Quant Imaging Med Surg*, 2021, **11**, 3494–3505.
52 G. A. Holzapfel, , DOI:10.1016/j.jtbi.2005.05.006ï.
53 S. Singh and M. Torzewski, *Biomolecules*, 2019, 9.
54 S. R. and E. Z. Khalil N. Bitar, 2015, **146**, 1614–1624.
55 B. Syeda, M. Gottsauner-Wolf, S. Denk, P. Pichler, A. Khorsand and D. Glogar, *Am J Hypertens*, 2003, **16**, 356–362.
56 N. Shashikanth, S. Yeruva, M. L. D. M. Ong, M. A. Odenwald, R. Pavlyuk and J. R. Turner, *Compr Physiol*, 2017, **7**, 1497–1518.
57 K. L. Edelblum and J. R. Turner, *Epithelial Cells: Structure, Transport, and Barrier Function*, Elsevier, Fourth Edi., 2015, vol. 1–2.
58 G. A. Holzapfel, T. C. Gasser and R. W. Ogden, *J Elast*, 2000, **61**, 1–48.
59 L. Claesson-Welsh, E. Dejana and D. M. McDonald, *Trends Mol Med*, 2021, **27**, 314–331.
60 M. Lasalvia, S. Castellani, P. D'Antonio, G. Perna, A. Carbone, A. L. Colia, A. B. Maffione, V. Capozzi and M. Conese, *Exp Cell Res*, 2016, **348**, 46–55.
61 S. K. Lai, Y.-Y. Wang, D. Wirtz and J. Hanes, *Adv Drug Deliv Rev*, 2009, **61**, 86–100.
62 M. A. Jankowska, M. Bartkowiak-Jowsa and R. Bedzinski, *J Mech Behav Biomed Mater*, 2015, **50**, 1–12.
63 B. Hoffman, M. Martin, B. N. Brown, L. J. Bonassar and J. Cheetham, *Laryngoscope*, 2015, 1–7.
64 J. K. Rains, J. L. Bert, C. R. Roberts and P. D. Pare, *J Appl Physiol*, 1992, **72**, 219–225.

65 L. Krupa, B. Bajka, R. Staroń, D. Dupont, H. Singh, K. Gutkowski and A. Macierzanka, *Sci Rep*, DOI:10.1038/s41598-020-77129-4.

66 Y. Lu, H. Wu, J. Li, Y. Gong, J. Ma, G. S. Kassab, Y. Huo, W. Tan and Y. Huo, *Sci Rep*, 2017, **7**, 1–12.

67 D. C. Stewart, D. Berrie, J. Li, X. Liu, C. Rickerson, D. Mkoji, A. Iqbal, S. Tan, A. L. Doty, S. C. Glover and C. S. Simmons, *PLoS One*, DOI:10.1371/journal.pone.0200377.

68 L. Wang, S. K. Murthy, G. A. Barabino and R. L. Carrier, *Biomaterials*, 2010, **31**, 7586–7598.

69 G. A. Holzapfel, G. Sommer, M. Auer, P. Regitnig and R. W. Ogden, *Ann Biomed Eng*, 2007, **35**, 530–545.

70 V. I. Egorov, I. V Schastlivtsev, E. V Prut, A. O. Baranov and R. A. Turusov, *J Biomech*, 2002, **35**, 1417–1425.

71 C.-C. Chou and J. M. Dabney, *Intestinal Compliance*, 1967, vol. 12.

72 F. V Brozovich, C. J. Nicholson, C. V Degen, Y. Z. Gao, M. Aggarwal and K. G. Morgan, 2016, 476–532.

73 J. Chen, T. Oshima, X. Huang, T. Tomita, H. Fukui and H. Miwa, *J Clin Med*, DOI:10.3390/jcm11144246.

74 H. Shen, X. Hu, H. Cui, Y. Zhuang, D. Huang, F. Yang, X. Wang, S. Wang and D. Wu, *J Mater Chem B*, 2016, **4**, 7689–7696.

75 M. Hassan, S. Aceves, R. Dohil, A. Gharibans, R. Newbury, J. Proudfoot and H. Mousa, *J Pediatr Gastroenterol Nutr*, 2019, **68**, 559–565.

76 J. Yang, J. Zhao, D. Liao and H. Gregersen, *J Biomech*, 2006, **39**, 894–904.

77 M. G. Dalghi, N. Montalbetti, M. D. Carattino and G. Apodaca, *Physiol Rev*.

78 H. O. Negrete, J. P. Lavelle, J. Berg, S. A. Lewis and M. L. Zeidel, *American Journal of Physiology-Renal Physiology*, 1996, **271**, F886–F894.

79 J. C. Mathai, E. H. Zhou, W. Yu, J. H. Kim, G. Zhou, Y. Liao, T. T. Sun, J. J. Fredberg and M. L. Zeidel, *Biophys J*, 2014, **107**, 1273–1279.

80 J. S. Walter, J. S. Wheeler, C. Morgan, P. Zaszczurynski and M. Plishka, *Neurourol Urodyn*, 1993, **12**, 273–276.

81 N. E. Vrana, P. Lavalle, M. R. Dokmeci, F. Dehghani, A. M. Ghaemmaghami and A. Khademhosseini, *Tissue Eng Part B Rev*, 2013, **19**, 529–543.

82 R. Saksena, C. Gao, M. Wicox and A. de Mel, *J Tissue Eng*, 2016, 7.

83 K. T. Callesen, A. Yuste-Montalvo, L. K. Poulsen, B. M. Jensen and V. Esteban, *Biomedicines*, , DOI:10.3390/biomedicines9040439.

84 N. Yu. Ignat'eva, N. A. Danilov, S. V. Averkiev, M. V. Obrezkova, V. V. Lunin and E. N. Sobol', *Journal of Analytical Chemistry*, 2007, **62**, 51–57.

85 C. M. Niessen, *Journal of Investigative Dermatology*, 2007, 127, 2525–2532.

86 M. N. Yu. Ignat'eva, NA Danilov, SV Averkiev, V. Obrezkova and Lunin, 2007, **62**, 59–65.

87 C. D. Devillard and C. A. Marquette, *Front Bioeng Biotechnol*, 2021, 9.
88 P. Jain, S. B. Rauer, M. Möller and S. Singh, *Biomacromolecules*, 2022, 23, 3081–3103.
89 G. A. Stooke-Vaughan and O. Campàs, *Curr Opin Genet Dev*, 2018, 51, 111–119.
90 N. Khalilgharibi and Y. Mao, *Open Biol*, 2021, 11.
91 Z. Wang, M. Li, B. Wang, Y. Xu, J. Li, S. Zhang, Q. Qin and J. Wang, *Chemical Engineering Journal*, 2023, **451**, 138805.
92 A. J. Engler, S. Sen, H. L. Sweeney and D. E. Discher, *Cell*, 2006, **126**, 677–689.
93 H. Schweikl, R. Müller, C. Englert, K. A. Hiller, R. Kujat, M. Nerlich and G. Schmalz, *J Mater Sci Mater Med*, 2007, **18**, 1895–1905.
94 M. Barrera-Velázquez and L. D. Ríos-Barrera, *Biol Open*, DOI:10.1242/bio.058760.
95 U. D. Jerman, M. E. Kreft and P. Veranič, *Tissue Eng Part B Rev*, 2015, 21, 521–530.
96 G. R. Cunha and L. Baskin, *Differentiation*, 2016, 91, 20–27.
97 Z.-M. Y. Ren-Qian Wei, Bo Tan, Mei-Yun Tan, Jing-Cong Luo, Li Deng, Xiao-He Chen, Xiu-Qun Li, Xiao Zuo, Wei Zhi, Peng Yang, Hui-Qi Xe, 2009, 453–461.
98 J. Zhang, J. Muri, G. Fitzgerald, T. Gorski, R. Gianni-Barrera, E. Masschelein, G. D'Hulst, P. Gilardoni, G. Turiel, Z. Fan, T. T. Wang, M. Planque, P. Carmeliet, L. Pellerin, C. Wolfrum, S. M. Fendt, A. Banfi, C. Stockmann, I. Soro-Arnáiz, M. Kopf and K. De Bock, *Cell Metab*, 2020, **31**, 1136-1153.e7.
99 R. Fitridge and M. Thompson, *Mechanisms of Vascular Disease*, Adelaide, 2011.
100 L. Liu, B. Stephens, M. Bergman, A. May and T. Chiang, 2021, 1–13.
101 B. R. Lee, R. I. Silver, A. W. Partin, J. I. Epstein and J. P. Gearhart, *Elsevier*.
102 T. J. McKee, G. Perlman, M. Morris and S. V. Komarova, *Sci Rep*, , DOI:10.1038/s41598-019-46896-0.
103 J. C. Ribeiro-Silva, P. Nolasco, J. E. Krieger and A. A. Miyakawa, *Int J Mol Sci*, DOI:10.3390/ijms221810175.
104 N. Shi and S. Y. Chen, *J Cell Physiol*, 2016, 231, 777–787.
105 B. C. Isenberg, C. Williams and R. T. Tranquillo, *Circ Res*, 2006, 98, 25–35.
106 M. Marzaro, M. Algeri, L. Tomao, S. Tedesco, T. Caldaro, V. Balassone, A. C. Contini, L. Guerra, G. F. D. Abriola, P. Francalanci, M. E. Caristo, L. Lupoi, I. Boskoski, A. Bozza, G. Astori, G. Pozzato, A. Pozzato, G. Costamagna and L. D. Oglio, 2020, 1–12.
107 J. Li, K. Zhang, W. Ma, F. Wu, P. Yang, Z. He and N. Huang, *Regen Biomater*, 2016, **1**, 149–157.
108 T. M. Do, Y. Yang and A. Deng, *Polymers (Basel)*, DOI:10.3390/polym13224042.
109 A. Ray, O. Lee, Z. Win, R. M. Edwards, P. W. Alford, D. H. Kim and P. P. Provenzano, *Nat Commun*, , DOI:10.1038/ncomms14923.

110 C. Parisi, B. Thiébot, G. Mosser, L. Trichet, P. Manivet and F. M. Fernandes, *Biomater Sci*, 2022, **10**, 6939–6950.

111 C. A. Dessalles, C. Leclech, A. Castagnino and A. I. Barakat, *Commun Biol*, 2021, **4**, 764.

112 K. Qin, C. Parisi and F. M. Fernandes, *J Mater Chem B*, 2021, **9**, 889–907.

113 K. Ławkowska, C. Rosenbaum, P. Petrasz, L. Kluth, K. Koper, T. Drewa, M. Pokrywczynska and J. Adamowicz, *Front Bioeng Biotechnol*, DOI:10.3389/fbioe.2022.1040987.

114 S. Bhargava, J. M. Patterson, R. D. Inman, S. MacNeil and C. R. Chapple, *Eur Urol*, 2008, **53**, 1263–1271.

115 A. I. Toma, J. M. Fuller, N. J. Willett and S. L. Goudy, *Translational Research*, 2021, 236, 17–34.

116 E. Maurizi, D. Adamo, F. M. Magrelli, G. Galaverni, E. Attico, A. Merra, M. B. R. Maffezzoni, L. Losi, V. G. Genna, V. Sceberras and G. Pellegrini, *Front Bioeng Biotechnol*, , DOI:10.3389/fbioe.2021.652214.

117 G. Ram-Liebig, J. Bednarz, B. Stuerzebecher, D. Fahlenkamp, G. Barbagli, G. Romano, U. Balsmeyer, M.-E. Spiegeler, S. Liebig and H. Knispel, *Adv Drug Deliv Rev*, 2015, **82–83**, 181–191.

118 G. Ram-Liebig, G. Barbagli, A. Heidenreich, D. Fahlenkamp, G. Romano, U. Rebmann, D. Standhaft, H. van Ahlen, S. Schakaki, U. Balsmeyer, M. Spiegeler and H. Knispel, *EBioMedicine*, 2017, **23**, 185–192.

119 Y. Xue, X. Cai, L. Wang, B. Liao, H. Zhang, Y. Shan, Q. Chen, T. Zhou, X. Li, J. Hou, S. Chen, R. Luo, D. Qin, D. Pei and G. Pan, *PLoS One*, DOI:10.1371/journal.pone.0070573.

120 J. Lu, L. F. Zhu, Y. M. Cai, H. Y. Dong, L. Zhu and J. M. Tan, *Mol Med Rep*, 2019, **19**, 187–194.

121 M. Culenova, A. Nicodemou, Z. V. Novakova, M. Debreova, V. Smolinská, S. Bernatova, D. Ivanisova, O. Novotna, J. Vasicek, I. Varga, S. Ziaran and L. Danisovic, *Int J Mol Sci*, , DOI:10.3390/ijms222212503.

122 H. Tian, S. Bharadwaj, Y. Liu, P. X. Ma, A. Atala and Y. Zhang, *Tissue Eng Part A*, 2010, **16**, 1769–1779.

123 K. Suzuki, M. Koyanagi-Aoi, K. Uehara, N. Hinata, M. Fujisawa and T. Aoi, *Sci Rep*, DOI:10.1038/s41598-019-46848-8.

124 Y. Inoue, T. Kishida, S. ichiro Kotani, M. Akiyoshi, H. Taga, M. Seki, O. Ukimura and O. Mazda, *Sci Rep*, DOI:10.1038/s41598-019-50388-6.

125 J. P. Koo, C. H. Kim, J. G. Lee, K. S. Kim and J. H. Yoon, *Laryngoscope*, 2007, **117**, 1750–1755.

126 L. Huu Dang, S.-H. Hung, Y. Tseng, L. Xuan Quang, N. Thao Ngoc Le, C.-L. Fang and H. Tseng, *International Journal of Molecular Sciences Article Int. J. Mol. Sci*, 2021, **22**, 10322.

127 M. Kanzaki, M. Yamato, H. Hatakeyama, C. Kohno, J. Yang, T. Umemoto, A. Kikuchi, T. Okano and T. Onuki, *Tissue Eng*, 2006, **12**, 1275–1283.

128 A. K. Saxena, H. Ainoedhofer and M. E. Höllwarth, *J Pediatr Surg*, 2009, **44**, 896–901.

129 T. Jensen, H. Wanczyk, I. Sharma, A. Mitchell, W. N. Sayej and C. Finck, *J Pediatr Surg*, 2019, **54**, 1744–1754.

130 T. Sato, R. G. Vries, H. J. Snippert, M. Van De Wetering, N. Barker, D. E. Stange, J. H. Van Es, A. Abo, P. Kujala, P. J. Peters and H. Clevers, *Nature*, 2009, **459**, 262–265.

131 J. Sprangers, I. C. Zaalberg and M. M. Maurice, *Cell Death Differ*, 2021, **28**, 95–107.

132 S. Yui, T. Nakamura, T. Sato, Y. Nemoto, T. Mizutani, X. Zheng, S. Ichinose, T. Nagaishi, R. Okamoto, K. Tsuchiya, H. Clevers and M. Watanabe, *Nat Med*, 2012, **18**, 618–623.

133 S. Sugimoto, Y. Ohta, M. Fujii, M. Matano, M. Shimokawa, K. Nanki, S. Date, S. Nishikori, Y. Nakazato, T. Nakamura, T. Kanai and T. Sato, *Cell Stem Cell*, 2018, **22**, 171-176.e5.

134 X. Luo, C. Han, P. Yang, A. Zhao, D. Zou, L. Jiang, P. Gao, B. Yin and N. Huang, *Colloids Surf B Biointerfaces*, , DOI:10.1016/j.colsurfb.2020.111307.

135 A. Fayon, D. Helle, G. Francius, J. B. Vincourt, V. Regnault, D. Dumas, P. Menu and R. El Omar, *Front Bioeng Biotechnol*, DOI:10.3389/fbioe.2022.884069.

136 T. Wu, J. Zhang, Y. Wang, B. Sun, M. Yin, G. L. Bowlin and X. Mo, *ACS Appl Bio Mater*, 2018, **1**, 833–844.

137 L. M. van den Boogaart, J. K. A. Langowski and G. J. Amador, *Biomimetics*, 2022, **7**, 134.

138 W. Li, Y. Zheng, W. Pang and P. Lai, *Biomedical Technology*, 2023, **1**, 65–72.

139 W. Xie, V. Kothari and B. S. Terry, *Biomed Microdevices*, DOI:10.1007/s10544-015-9972-7.

140 C. Xu, Y. Chen, Y. Si, Y. Yan, A. B. Kayitmazer, Y. Ding, W. Qian, Z. Zheng, S. Cao and Y. Xu, *Adv Mater Interfaces*, , DOI:10.1002/admi.202001955.

141 R. R. Pillai and V. Thomas, *Polymers (Basel)*, 2023, 15.

142 Y. Jiang, H. Wang, X. Wang and Q. Li, *Int J Biol Macromol*, 2022, **219**, 1146–1154.

143 H. Lai, B. Gong, J. Yin and J. Qian, *Mater Des*, 2022, **218**, 110663.

144 M. F. A. Cutiongco, S. H. Goh, R. Aid-Launais, C. Le Visage, H. Y. Low and E. K. F. Yim, *Biomaterials*, 2016, **84**, 184–195.

145 S. Yunoki, E. Kondo and K. Yasuda, in *Collagen Biomaterials*, IntechOpen, 2022.

146 J. Hu, B. Ai, S. Zhu, Z. Wang, H. Xia and W. Jia, *J Biomater Appl*, 2022, **36**, 956–964.

147 O. A. Romanova, T. H. Tenchurin, T. S. Demina, E. V. Sytina, A. D. Shepelev, S. G. Rudyak, O. I. Klein, S. V. Krasheninnikov, E. I. Safronova, R. A. Kamyshinsky, V. G. Mamagulashvili, T. A. Akopova, S. N. Chvalun and A. A. Panteleyev, *Cell Prolif*, , DOI:10.1111/cpr.12598.

148 P. Jain, S. B. Rauer, M. Möller and S. Singh, *Biomacromolecules*, 2022, **23**, 3081–3103.

149 K. Zhang, M. A. Bhutto, L. Wang, K. Wang, J. Liu, W. Li, W. Cui and Q. Fu, *Advanced Fiber Materials*, 2023, **5**, 662–680.

150 J. A. Reid and A. Callanan, *J Biomed Mater Res B Appl Biomater*, 2020, **108**, 910–924.

151 J. Dolgin, S. N. Hanumantharao, S. Farias, C. G. Simon and S. Rao, *Fibers*, 2023, **11**, 39.

152 Y. Niu, M. Galluzzi, M. Fu, J. Hu and H. Xia, *J Nanobiotechnology*, DOI:10.1186/s12951-021-01091-0.

153 D. Dems, J. Rodrigues Da Silva, C. Hélary, F. Wien, M. Marchand, N. Debons, L. Muller, Y. Chen, M. C. Schanne-Klein, C. Laberty-Robert, N. Krins and C. Aimé, *ACS Appl Bio Mater*, 2020, **3**, 2948–2957.

154 M. Ghosh, S. Ahmad, C. W. White and S. D. Reynolds, *Am J Respir Cell Mol Biol*, 2017, **56**, 1–10.

155 H. A. Khalil, S. N. Hong, J. D. Rouch, A. Scott, Y. Cho, J. Wang, M. S. Lewis, M. G. Martin, J. C. Y. Dunn and M. G. Stelzner, *PLoS One*, 2019, **14**, e0216326.

156 G. Barbagli, I. Akbarov, A. Heidenreich, V. Zugor, R. Olianas, M. Aragona, G. Romano, U. Balsmeyer, D. Fahlenkamp, U. Rebmann, D. Standhaft and M. Lazzeri, *Journal of Urology*, 2018, **200**, 448–456.

157 G. Bento, A. K. Shafigullina, A. A. Rizvanov, V. A. Sardão, M. P. Macedo and P. J. Oliveira, *Cells*, 2020, **9**, 573.

158 Samuel S. Hinman, Yuli Wang, Raehyun Kim and Nancy L. Allbritton, *Nat Protoc*, 2021, **16**, 352–382.

159 E. Elia, D. Brownell, S. Chabaud and S. Bolduc, *Int J Mol Sci*, 2022, **24**, 9.

160 A. Atala, F. Kurtis Kasper and A. G. Mikos, *Sci Transl Med*, DOI:10.1126/scitranslmed.3004890.

161 A. Porzionato, E. Stocco, S. Barbon, F. Grandi, V. Macchi and R. De Caro, *Int J Mol Sci*, 2018, **19**, 4117.

162 L. P. Frazão, A. M. Fernandes, C. Oliveira, A. Martins, T. H. Silva, J. Vieira De Castro, C. Nogueira-Silva and N. M. Neves, *ACS Biomater Sci Eng*, 2021, **7**, 3423–3433.

163 E. Martinod, K. Chouahnia, D. M. Radu, P. Joudiou, Y. Uzunhan, M. Bensidhoum, A. M. Santos Portela, P. Guiraudet, M. Peretti, M. D. Destable, A. Solis, S. Benachi, A. Fialaire-Legendre, H. Rouard, T. Collon, J. Piquet, S. Leroy, N. Vénissac, J. Santini, C. Tresallet, H. Dutau, G. Sebbane, Y. Cohen, S. Beloucif, A. C. D'Audiffret, H. Petite, D. Valeyre, A. Carpentier and E. Vicaut, *JAMA - Journal of the American Medical Association*, 2018, **319**, 2212–2222.

164 S. F. Badylak, B. Kropp, T. Mcpherson, H. Liang and P. W. Snyder, *Tissue Eng*.

165 T. W. Jernigan, M. A. Croce, C. Cagiannos, D. H. Shell, C. R. Handorf, T. C. Fabian, D. V. Feliciano, E. E. Cornwell and B. A. Pruitt, *Ann Surg*, 2004, **239**, 733–740.

166 J. Negishi, Y. Hashimoto, A. Yamashita, Y. Zhang, T. Kimura, A. Kishida and S. Funamoto, *J Biomed Mater Res A*, 2017, **105**, 1293–1298.

167 Q. Xu, C. Chen, Z. Xu, F. Chen, Y. Yu, X. Hong, S. Xu, J. Chen, Q. Ding and H. Chen, *Asian J Urol*, 2020, **7**, 51–55.

168 G. Totonelli, P. Maghsoudlou, J. M. Fishman, G. Orlando, T. Ansari, P. Sibbons, M. A. Birchall, A. Pierro, S. Eaton and P. De Coppi, *World J Gastroenterol*, 2012, **18**, 6900–6907.

169 Y. Takimoto, T. Nakamura, Y. Yamamoto, T. Kiyotani, M. Teramachi and Y. Shimizu, *General thoracic surgery*.

170 M. A. Rodríguez-Soto, C. A. Polanía-Sandoval, A. M. Aragón-Rivera, D. Buitrago, M. Ayala-Velásquez, A. Velandia-Sánchez, G. Peralta Peluffo, J. C. Cruz, C. Muñoz Camargo, J. Camacho-Mackenzie, J. G. Barrera-Carvajal and J. C. Briceño, *Polymers (Basel)*, 2022, 14.

171 H. Omid, S. Abdollahi, S. Bonakdar, N. Haghighipour, M. A. Shokrgozar and J. Mohammadi, *J Mater Sci Mater Med*, DOI:10.1007/s10856-023-06716-4.

172 O. M. El-Taji, A. Q. Khattak and S. A. Hussain, *Oncol Lett*, 2015, 3–10.

173 M. Garriboli, K. Deguchi, G. Totonelli, F. Georgiades, L. Urbani, M. Ghionzoli, A. J. Burns, N. J. Sebire, M. Turmaine, S. Eaton and P. De Coppi, *Pediatr Surg Int*, 2022, **38**, 665–677.

174 Y. Zhang, X. S. Li, A. G. Guex, S. S. Liu, E. Müller, R. I. Malini, H. J. Zhao, M. Rottmar, K. Maniura-Weber, R. M. Rossi and F. Spano, *Biofabrication*, , DOI:10.1088/1758-5090/aa6bae.

175 F. Zhang, T. Bambharoliya, Y. Xie, L. Liu, H. Celik, L. Wang, W. College and N. Carolina, *Materials Science & Engineering C*, DOI:10.1016/j.msec.2020.111418.

176 L. Magnan, G. Labrunie, M. Fénelon, N. Dusserre, M. P. Foulc, M. Lafourcade, I. Svahn, E. Gontier, J. H. Vélez V., T. N. McAllister and N. L'Heureux, *Acta Biomater*, 2020, **105**, 111–120.

177 F. Gobeaux, Université Pierre et Marie Curie, 2008.

178 P. Kuppan, S. Sethuraman and U. M. Krishnan, *J Biomed Mater Res A*, 2015, **103**, 2236–2250.

179 H. A. Strobel, E. L. Calamari, A. Beliveau, A. Jain and M. W. Rolle, *J Biomed Mater Res B Appl Biomater*, 2018, **106**, 817–826.

180 X. Lu, H. Zou, X. Liao, Y. Xiong, X. Hu, J. Cao, J. Pan, C. Li and Y. Zheng, *Biomedical Materials (Bristol)*, , DOI:10.1088/1748-605X/aca269.

181 D. G. Simpson, B. S. Jha, C. E. Ayres, J. R. Bowman, T. A. Telemeco, S. A. Sell and G. L. Bowlin, *J Nanomater*, DOI:10.1155/2011/348268.

182 B. N. Blackstone, S. C. Gallentine and H. M. Powell, *Bioengineering*, 2021, **8**, 39.

183 J. Venugopal, L. L. Ma, T. Yong and S. Ramakrishna, *Cell Biol Int*, 2005, **29**, 861–867.

184 T. Wu, J. Zhang, Y. Wang, B. Sun, M. Yin, G. L. Bowlin and X. Mo, *ACS Appl Bio Mater*, 2018, **1**, 833–844.

185 I. Roy and M. N. Gupta, *Biotechnol Appl Biochem*, 2004, **39**, 165–177.

186 R. Polak and R. N. M. Pitombo, *Cryobiology*, 2011, **63**, 61–66.

187 D. I. Zeugolis, S. T. Khew, E. S. Y. Yew, A. K. Ekaputra, Y. W. Tong, L. Y. L. Yung, D. W. Hutmacher, C. Sheppard and M. Raghunath, *Biomaterials*, 2008, **29**, 2293–2305.

188 A. Elamparithi, A. M. Punnoose and S. Kuruvilla, *Artif Cells Nanomed Biotechnol*, 2016, **44**, 1318–1325.

189 J. A. Matthews, G. E. Wnek, D. G. Simpson and G. L. Bowlin, *Biomacromolecules*, 2002, **3**, 232–238.

190 U. G. K. Wegst, M. Schecter, A. E. Donius and P. M. Hunger, *Philosophical Transactions of the Royal Society A: Mathematical, Physical and Engineering Sciences*, 2010, **368**, 2099–2121.

191 S. Deville, E. Saiz and A. P. Tomsia, *Acta Mater*, 2007, **55**, 1965–1974.

192 V. Kocherbitov, *Carbohydr Polym*, 2016, **150**, 353–358.

193 K. Qin, C. Eschenbrenner, F. Ginot, D. Dedovets, T. Coradin, S. Deville and F. M. Fernandes, *Journal of Physical Chemistry Letters*, 2020, **11**, 7730–7738.

194 L. Buttafoco, A. A. Poot, P. J. Dijkstra, W. F. Daamen, T. H. Van Kuppevelt, I. Vermes and J. Feijen, 2005, 357–368.

195 I. Martinier, F. Fage, A. Kakar, A. Castagnino, E. Saindoy, J. Frederick, I. Onorati, V. Besnard, A. I. Barakat, N. Dard, E. Martinod, C. Planes, L. Trichet and F. M. Fernandes, *biorXiv*, DOI:10.1101/2023.08.30.555553.

196 J. Seuba, J. Leloup, S. Richaud, S. Deville, C. Guizard and A. J. Stevenson, *J Eur Ceram Soc*, 2017, **37**, 2423–2429.

197 H. Joukhdar, A. Seifert, T. Jüngst, J. Groll, M. S. Lord and J. Rnjak-Kovacina, *Advanced Materials*, DOI:10.1002/adma.202100091.

198 D. Dedovets, C. Monteux and S. Deville, *Science (1979)*, 2018, 303–306.

199 J. A. Cyr, A. Husmann, S. M. Best and R. E. Cameron, *Acta Biomater*, 2022, **153**, 260–272.

200 M. Marcellini, C. Noirjean, D. Dedovets, J. Maria and S. Deville, *ACS Omega*, 2016, **1**, 1019–1026.

201 K. M. Pawelec, A. Husmann, S. M. Best and R. E. Cameron, *Appl Phys Rev*, , DOI:10.1063/1.4871083.

202 C. Rieu, C. Parisi, G. Mosser, B. Haye, T. Coradin, F. M. Fernandes and L. Trichet, *ACS Appl Mater Interfaces*, 2019, **11**, 14672–14683.

203 M. C. Gutiérrez, M. L. Ferrer and F. Del Monte, *Chemistry of Materials*, 2008, **20**, 634–648.

204 M. W. Pot, K. A. Faraj, A. Adawy, W. J. P. Van Enckevort, H. T. B. Van Moerkerk, E. Vlieg, W. F. Daamen and T. H. Van Kuppevelt, *ACS Appl Mater Interfaces*, 2015, **7**, 8495–8505.

205 X. Liu and P. X. Ma, *Biomaterials*, 2009, **30**, 4094–4103.

206 J. Lee and G. Kim, *ACS Appl Mater Interfaces*, 2018, **10**, 35801–35811.

207 H. W. Liu, W. T. Su, C. Y. Liu and C. C. Huang, *Int J Mol Sci*, , DOI:10.3390/ijms23158449.

208 J. L. Zitnay, S. P. Reese, G. Tran, N. Farhang, R. D. Bowles and J. A. Weiss, *Acta Biomater*, 2018, **65**, 76–87.

209 C. Katrilaka, N. Karipidou, N. Petrou, C. Manglaris, G. Katrilakas, A. N. Tzavellas, M. Pitou, E. E. Tsiridis, T. Choli-Papadopoulou and A. Aggeli, *Materials*, 2023, **16**, 4425.

210 K. Yin, P. Divakar and U. G. K. Wegst, *Acta Biomater*, 2019, **84**, 231–241.

211 P. Divakar, K. Yin and U. G. K. Wegst, *J Mech Behav Biomed Mater*, 2019, **90**, 350–364.

212 N. Davidenko, C. F. Schuster, D. V. Bax, N. Raynal, R. W. Farndale, S. M. Best and R. E. Cameron, *Acta Biomater*, 2015, **25**, 131–142.

213 D. K. Chang, M. R. Louis, A. Gimenez and E. M. Reece, *Semin Plast Surg*, 2019, **33**, 185–189.

214 O. Kloeters, F. Unglaub, E. de Laat, M. van Abeelen and D. Ulrich, *Int Wound J*, 2016, **13**, 1231–1236.

215 J. H. Min, I. S. Yun, D. H. Lew, T. S. Roh and W. J. Lee, *Arch Plast Surg*, 2014, **41**, 330–336.

216 S. Govender, C. Csimma, H. K. Genant and A. Valentin-Opran, *J Bone Joint Surg*, 2002, **84-A**, 2123–2134.

217 P. K. Narotam, S. José, N. Nathoo, C. Taylon and Y. Vora, *Spine (Phila Pa 1976)*, 2004, **29**, 2861–2867.

218 X. Cao, S. Maharjan, R. Ashfaq, J. Shin and Y. S. Zhang, *Engineering*, 2021, **7**, 832–844.

219 Y.-C. Hou, X. Cui, Z. Qin, C. Su, G. Zhang, J.-N. Tang, J.-A. Li and J.-Y. Zhang, *Int J Bioprint*, 2023, **9**, 0.

220 F. Pati, J. Jang, D.-H. Ha, S. Won Kim, J.-W. Rhie, J.-H. Shim, D.-H. Kim and D.-W. Cho, *Nat Commun*, 2014, **5**, 3935.

221 K. Dzobo, K. S. C. M. Motaung and A. Adesida, *Int J Mol Sci*, 2019, **20**, 4628.

222 Z. Y. Xu, J. J. Huang, Y. Liu, C. W. Chen, G. W. Qu, G. F. Wang, Y. Zhao, X. W. Wu and J. A. Ren, *Bioeng Transl Med*, DOI:10.1002/btm2.10327.

223 Y. Zhao, Y. Liu, Y. Dai, L. Yang and G. Chen, *Micromachines (Basel)*, 2022, **13**, 1073.

224 C. Norotte, F. S. Marga, L. E. Niklason and G. Forgacs, *Biomaterials*, 2009, **30**, 5910–5917.

225 M. M. De Santis, H. N. Alsafadi, S. Tas, D. A. Bölükbas, S. Prithiviraj, I. A. N. Da Silva, M. Mittendorfer, C. Ota, J. Stegmayr, F. Daoud, M. Königshoff, K. Swärd, J. A. Wood, M. Tassieri, P. E. Bourgine, S. Lindstedt, S. Mohlin and D. E. Wagner, *Advanced Materials*, DOI:10.1002/adma.202005476.

226 G. Gao, J. H. Lee, J. Jang, D. H. Lee, J. Kong, B. S. Kim, Y. Choi, W. B. Jang, Y. J. Hong, S. Kwon and D. Cho, *Adv Funct Mater*, DOI:10.1002/adfm.201700798.

227 Z. Wang, L. Wang, T. Li, S. Liu, B. Guo, W. Huang and Y. Wu, *Theranostics*, 2021, **11**, 7948–7969.

228 S. Liu, T. Wang, S. Li and X. Wang, *Polymers (Basel)*, 2022, **14**, 2182.

229 A. Lee, A. R. Hudson, D. J. Shiwarski, J. W. Tashman, T. J. Hinton, S. Yerneni, J. M. Bliley, P. G. Campbell and A. W. Feinberg, *Science (1979)*, 2019, **365**, 482–487.

230 C. Z. Liu, Z. D. Xia, Z. W. Han, P. A. Hulley, J. T. Triffitt and J. T. Czernuszka, *J Biomed Mater Res B Appl Biomater*, 2008, **85**, 519–528.

231 Y. B. Kim, H. Lee and G. H. Kim, *ACS Appl Mater Interfaces*, 2016, **8**, 32230–32240.

232 M. K. Włodarczyk-Biegun and A. del Campo, *Biomaterials*, 2017, **134**, 180–201.

233 H. Suo, J. Zhang, M. Xu and L. Wang, *Materials Science and Engineering C*, DOI:10.1016/j.msec.2021.111963.

234 A. Nagaraj, A. E. Etxeberria, R. Naffa, G. Zidan and A. Seyfoddin, *Biology (Basel)*, 2022, **11**, 1561.

235 S. O. Sarrigiannidis, J. M. Rey, O. Dobre, C. González-García, M. J. Dalby and M. Salmeron-Sanchez, *Mater Today Bio*, 2021, **10**, 100098.

236 E. O. Osidak, V. I. Kozhukhov, M. S. Osidak and S. P. Domogatsky, *Int J Bioprint*, 2020, **6**, 270.

237 A. D. Nocera, R. Comín, N. A. Salvatierra and M. P. Cid, *Biomed Microdevices*, , DOI:10.1007/s10544-018-0270-z.

238 M. Camman, P. Joanne, J. Brun, A. Marcellan, J. Dumont, O. Agbulut and C. Hélary, *Biomaterials Advances*, DOI:10.1016/j.bioadv.2022.213219.

239 W. L. Ng, M. H. Goh, W. Y. Yeong and M. W. Naing, *Biomater Sci*, 2018, **6**, 562–574.

240 S. Shakibania, L. Ghazanfari, M. Raeeszadeh-Sarmazdeh and M. Khakbiz, *Drug Dev Ind Pharm*, 2021, **47**, 521–534.

241 M. Adamkiewicz and B. Rubinsky, *Cryobiology*, 2015, **71**, 518–521.

242 G. Kim, S. Ahn, H. Yoon, Y. Kim and W. Chun, *J Mater Chem*, 2009, **19**, 8817–8823.

243 A. Moghanizadeh, *Manuf Lett*, 2022, **31**, 116–118.

244 A. Garg, S. S. Yerneni, P. Campbell, P. R. LeDuc and O. B. Ozdoganlar, *Advanced Science*, DOI:10.1002/advs.202201566.

245 C. Wang, Q. Zhao and M. Wang, *Biofabrication*, , DOI:10.1088/1758-5090/aa71c9.

246 B. Stolz, M. Mader, L. Volk, T. Steinberg and R. Mülhaupt, *Macromol Mater Eng*, , DOI:10.1002/mame.202000541.

247 T. Liu, B. Yang, W. Tian, X. Zhang and B. Wu, *Polymers (Basel)*, , DOI:10.3390/polym14091722.

248 W. Zhang, I. Ullah, L. Shi, Y. Zhang, H. Ou, J. Zhou, M. W. Ullah, X. Zhang and W. Li, *Mater Des*, 2019, **180**, 107946.

249 Z. Tan, C. Parisi, L. Di Silvio, D. Dini and A. E. Forte, *Sci Rep*, , DOI:10.1038/s41598-017-16668-9.

250 M. Yamanami, K. Kanda, T. Kawasaki, D. Kami, T. Watanabe, S. Gojo and H. Yaku, *Artif Organs*, 2019, **43**, 773–779.

251 T. Shin'oka, Y. Imai and Y. Ikada, *New England Journal of Medicine*, 2001, **344**, 532–533.

252 B. Patel, Z. Xu, C. B. Pinnock, L. S. Kabbani and M. T. Lam, *Sci Rep*, 2018, **8**, 1–13.

253 N. L'Heureux, N. Dusserre, G. Konig, B. Victor, P. Keire, T. N. Wight, N. A. F. Chronos, A. E. Kyles, C. R. Gregory, G. Hoyt, R. C. Robbins and T. N. Mcallister, *Nat. Med.*, 2006, **12**, 361–365.

254 R. Gauvin, T. Ahsan, D. Larouche, P. Lé, J. Dubé, F. O. A. Auger, R. M. Nerem and L. Germain, *Tissue Eng Part A*.

255 W. Jakubowska, S. Chabaud, I. Saba, T. Galbraith, F. Berthod and S. Bolduc, *Tissue Eng Part A*, 2020, **26**, 811–822.

256 C. Caneparo, S. Chabaud, J. Fradette and S. Bolduc, *Sci Rep*, , DOI:10.1038/s41598-022-25311-1.

257 W. Xu, M. Yao, M. He, S. Chen and Q. Lu, *ACS Appl Mater Interfaces*, 2023, **15**, 19966–19975.

258 C. B. Pinnock, E. M. Meier, N. N. Joshi, B. Wu and M. T. Lam, *Methods*, 2016, **99**, 20–27.

259 A. W. Justin, F. Cammarata, A. A. Guy, S. R. Estevez, S. Burgess, H. Davaapil, A. Stavropoulou-Tatla, J. Ong, A. G. Jacob, K. Saeb-Parsy, S. Sinha and A. E. Markaki, *Biomaterials Advances*, 2023, **145**, 213245.

260 S. Malladi, D. Miranda-Nieves, L. Leng, S. J. Grainger, C. Tarabanis, A. P. Nesmith, R. Kosaraju, C. A. Haller, K. K. Parker, E. L. Chaikof and A. Günther, *ACS Biomater Sci Eng*, 2020, **6**, 4236–4246.

261 C. Loy, A. Lainé and D. Mantovani, *Biotechnol J*, 2016, **11**, 1673–1679.

262 Y. Huo, Y. Xu, X. Wu, E. Gao, A. Zhan, Y. Chen, Y. Zhang, Y. Hua, W. Swieszkowski, Y. S. Zhang and G. Zhou, *Advanced Science*, DOI:10.1002/advs.202202181.

263 H. Nam, H. J. Jeong, Y. Jo, J. Y. Lee, D. H. Ha, J. H. Kim, J. H. Chung, Y. S. Cho, D. W. Cho, S. J. Lee and J. Jang, *Sci Rep*, , DOI:10.1038/s41598-020-64049-6.

264 E. Bosch-Rué, L. M. Delgado, F. J. Gil and R. A. Perez, *Biofabrication*, DOI:10.1088/1758-5090/abbd27.

265 N. Diamantides, C. Dugopolski, E. Blahut, S. Kennedy and L. J. Bonassar, *Biofabrication*, DOI:10.1088/1758-5090/ab3524.

266 Y. Takeoka, K. Matsumoto, D. Taniguchi, T. Tsuchiya, R. Machino, M. Moriyama, S. Oyama, T. Tetsuo, Y. Taura, K. Takagi, T. Yoshida, A. Elgalad, N. Matsuo, M. Kunizaki, S. Tobinaga, T. Nonaka, S. Hidaka, N. Yamasaki, K. Nakayama and T. Nagayasu, *PLoS One*, DOI:10.1371/journal.pone.0211339.

267 Z. Li, C. Ruan and X. Niu, *Med Nov Technol Devices*, 2023, **17**, 100211.

268 L. R. Versteegden, K. A. van Kampen, H. P. Janke, D. M. Tiemessen, H. R. Hoogenkamp, T. G. Hafmans, E. A. Roozen, R. M. Lomme, H. van Goor, E. Oosterwijk, W. F. Feitz, T. H. van Kuppevelt and W. F. Daamen, *Acta Biomater*, 2017, **52**, 1–8.

269 X. Zhou, M. Nowicki, H. Sun, S. Y. Hann, H. Cui, T. Esworthy, J. D. Lee, M. Plesniak and L. G. Zhang, *ACS Appl Mater Interfaces*, , DOI:10.1021/acsami.0c14871.

270 J. M. Lee, S. K. Q. Suen, W. L. Ng, W. C. Ma and W. Y. Yeong, *Macromol Biosci*, DOI:10.1002/mabi.202000280.

271 Q. Pi, S. Maharjan, X. Yan, X. Liu, B. Singh, A. M. van Genderen, F. Robledo-Padilla, R. Parra-Saldivar, N. Hu, W. Jia, C. Xu, J. Kang, S. Hassan, H. Cheng, X. Hou, A. Khademhosseini and Y. S. Zhang, *Advanced Materials*, , DOI:10.1002/adma.201706913.

272 W. Kim and G. Kim, *ACS Appl Mater Interfaces*, 2018, **10**, 41185–41196.

273 Y. Xu, D. Li, Z. Yin, A. He, M. Lin, G. Jiang, X. Song, X. Hu, Y. Liu, J. Wang, X. Wang, L. Duan and G. Zhou, *Acta Biomater*, 2017, **58**, 113–121.

274 B. C. Isenberg, C. Williams and R. T. Tranquillo, *Circ Res*, 2006, **98**, 25–35.

275 M. Kamaraj, P. S. Giri, S. Mahapatra, F. Pati and S. N. Rath, *Int J Biol Macromol*, 2022, **223**, 1405–1419.

276 P. Maghsoudlou, G. Totonelli, S. P. Loukogeorgakis, S. Eaton and P. De Coppi, *J Vis Exp*, , DOI:10.3791/50658.

277 F. Grandi, E. Stocco, S. Barbon, A. Rambaldo, M. Contran, F. Fascetti Leon, P. Gamba, P. P. Parnigotto, V. Macchi, R. De Caro and A. Porzionato, *Biomed Res Int*, DOI:10.1155/2018/7824757.

278 G. Luc, G. Charles, C. Gronnier, M. Cabau, C. Kalisky, M. Meulle, R. Bareille, S. Roques, L. Couraud, J. Rannou, L. Bordenave, D. Collet and M. Durand, *Biomaterials*, 2018, **175**, 1–18.

279 S. Barbon, A. Biccari, E. Stocco, G. Capovilla, E. D'Angelo, M. Todesco, D. Sandrin, A. Bagno, F. Romanato, V. Macchi, R. De Caro, M. Agostini, S. Merigliano, M. Valmasoni and A. Porzionato, *Cells*, DOI:10.3390/cells11192945.

280 M. Garriboli, K. Deguchi, G. Totonelli, F. Georgiades, L. Urbani, M. Ghionzoli, A. J. Burns, N. J. Sebire, M. Turmaine, S. Eaton and P. De Coppi, *Pediatr Surg Int*, 2022, **38**, 665–677.

281 Y. Zhang, X. S. Li, A. G. Guex, S. S. Liu, E. Müller, R. I. Malini, H. J. Zhao, M. Rottmar, K. Maniura-Weber, R. M. Rossi and F. Spano, *Biofabrication*, 2017, **9**, 029501.

282 O. Syed, J.-H. Kim, Z. Keskin-Erdogan, R. M. Day, A. El-Fiqi, H.-W. Kim and J. C. Knowles, *Acta Biomater*, 2019, **99**, 181–195.

283 A. J. Ryan, E. J. Ryan, A. R. Cameron and F. J. O'Brien, *Acta Biomater*, 2020, **112**, 52–61.

284 M. Tamaddon, R. S. Walton, D. D. Brand and J. T. Czernuszka, *J Mater Sci Mater Med*, 2013, **24**, 1153–1165.

285 Z. Nematollahi, M. Tafazzoli-Shadpour, A. Zamanian, A. Seyedsalehi, S. Mohammad-Behgam, F. Ghorbani and F. Mirahmadi, *Iran Biomed J*, 2017, **21**, 228–239.

286 V. Shabafrooz, M. Mozafari, G. A. Köhler, S. Assefa, D. Vashaee and L. Tayebi, *J Biomed Mater Res A*, 2014, **102**, 3130–3139.

287 M. Saito, T. Sakamoto, M. Fujimaki, K. Tsukada, T. Honda and M. Nozaki, *Surg Today*.

288 M. B. Chan-Park, J. Y. Shen, Y. Cao, Y. Xiong, Y. Liu, S. Rayatpisheh, G. C. Kang and H. P. Greisler, *J Biomed Mater Res A*, 2009, **88A**, 1104–1121.

289 M. Yang, J. Chen, Y. Chen, W. Lin, H. Tang, Z. Fan, L. Wang, Y. She, F. Jin, L. Zhang, W. Sun and C. Chen, *Adv Healthc Mater*, , DOI:10.1002/adhm.202202022.

290 Y. Kobayashi, C. E. J. Cordonier, Y. Noda, F. Nagase, J. Enomoto, T. Kageyama, H. Honma, S. Maruo and J. Fukuda, *Sci Rep*, , DOI:10.1038/s41598-019-46801-9.

291 H. Okuyama, S. Umeda, Y. Takama, T. Terasawa and Y. Nakayama, *J Pediatr Surg*, 2018, **53**, 223–226.

292 F. Fazal, F. J. Diaz Sanchez, M. Waqas, V. Koutsos, A. Callanan and N. Radacsi, *Med Eng Phys*, 2021, **94**, 52–60.

293 J. H. Park, M. Ahn, S. H. Park, H. Kim, M. Bae, W. Park, S. J. Hollister, S. W. Kim and D. W. Cho, *Biomaterials*, DOI:10.1016/j.biomaterials.2021.121246.

294 J. Y. Park, H. Ryu, B. Lee, D. H. Ha, M. Ahn, S. Kim, J. Y. Kim, N. L. Jeon and D. W. Cho, *Biofabrication*, DOI:10.1088/1758-5090/aae545.

295 W. Farhat, F. Chatelain, A. Marret, L. Faivre, L. Arakelian, P. Cattan and A. Fuchs, *Biomaterials*, 2021, **267**, 120465.

296 A. R. Raji and M. Naserpour, *Journal of Veterinary Medicine Series C: Anatomia Histologia Embryologia*, 2007, **36**, 10–13.

297 P. K. Jeffery and L. Reid, *J. Anat*, 1975, **120**, 295–320.

298 J. M. Frasca, O. Auerbach, V. R. Parks and J. D. Jamieson, *Exp Mol Pathol*, 1968, 363–379.

299 W. S. Kim, J. W. Chang, W. S. Jang, Y. J. Seo, M. L. Kang, H. J. Sung, D. H. Kim, J. M. Kim, J. H. Park, M. J. Ban, G. Na, S. H. Shin, H. K. Byeon, Y. W. Koh, S. H. Kim, H. K. Baik and E. C. Choi, *Sci Rep*, DOI:10.1038/s41598-017-10733-z.